In vitro effects of 2-methoxyestradiol on morphology, cell cycle progression, cell death and gene expression changes in the tumorigenic MCF-7 breast epithelial cell line

Authors: B.A. Stander[a], S. Marais[a], C.J.J. Vorster[a] and A.M. Joubert[a]

[a] Department of Physiology, University of Pretoria, Pretoria, South Africa

1. Introduction

2-Methoxyestradiol (2ME) is an endogenous metabolite of 17β-estradiol exerting both antiangiogenic and antimitogenic effects *in vitro* and *in vivo* [1]. 2ME is a target for 17β-hydroxysteroid dehydrogenase-mediated metabolism that explains its low bioavailability due to rapid metabolic breakdown [2]. Results from preclinical tumor models in animals suggest that maintaining a plasma concentration of 2ME in the range of 3-17ng/ml (10-56nM) is needed for efficient anti-tumor activity [3-4]. 2ME is registered as Panzem^{R} by Entremed, Inc. (Rockville, MD) and is currently being used in clinical trials by making use of a novel nanocrystal dispersion (NCD) drug delivery system [5]. The NCD formulation of 2ME was shown to have improved bioavailability resulting in plasma concentration levels within the range needed for anti-tumor activity [3].

2ME plays as role in the abrogation of microtubule dynamics and the inhibition of protein translation and activity of the anaphase-promoting complex (APC/C) [6]. 2ME inhibits angiogenesis by interacting with endothelial tubulin dynamics which in turn negatively affects the expression and activity of hypoxia-inducible factor 1-alpha (HIF-1a) and vascular endothelial growth factor (VEGF) [7-8]. 2ME can also induce antiangiogenic effects through apoptosis as a result of increased phosphorylation of protein kinase B (Akt), activation of c-*jun* N-terminal- (JNK), extracellular signal-regulated- (ERK) and p38-kinases, activation of the intrinsic apoptotic pathway through inactivation of B-cell lymphoma 2 (Bcl-2) and Bcl-xL proteins as well as the upregulating the extrinsic pathway by increasing the expression of death receptor 5 (DR5) leading to activation of caspase-8 [6, 8-14]. Fukui and Zhu (2008) demonstrated that 2ME induced the phosphorylation of Bcl-2 proteins, but did not significantly alter the levels of Bcl-2-associated X protein (Bax) and Bcl-2 expression in MDA-MB-435 M14 melanoma derived metastatic cells [13, 15]. This is in contrast to the results found by Joubert *et al*. (2005) wherein 2ME altered the ratio of Bax/Bcl-2 expression levels in esophageal

cancer cells and cervical carcinoma cells [16-17]. In addition, 2ME induces apoptosis through the p38 pathway and not the JNK pathway in ovarian carcinoma cells, but activates and induces apoptosis through both the JNK and p38 pathways in prostate cancer cells [18-19]. MCF-7 cells are known to be caspase-3 deficient, since they do not express the CASP-3 gene as a result of a 47-base pair deletion within exon 3 of the gene, thus causing abrogated translation of CASP-3 mRNA [20]. These observations, among others, indicate that the mechanism of action of 2ME-induced growth inhibition is cell line specific.

Since the exact mechanism of 2ME's action is cell line specific and remains to be elucidated, the purpose of this study was to investigate the *in vitro* influence of 2ME in the MCF-7 breast adenocarcinoma cell line. The MCF-7 cell line is a tumorigenic estrogen receptor positive breast cell line that lacks caspase 3 expression [20]. Data obtained from the influence of 2ME on cyclin B1 levels, its effect on the release of cytochrome *c*, the generation of reactive oxygen species, as well as information obtained from its influence on global gene expression further contribute to the mechanism exerted by 2ME on tumorigenic breast cancer cells. In addition, a novel finding namely the induction of both apoptosis and autophagy as a possible combination of types of cell death induced by 2ME in MCF-7 cells is proposed.

2. Materials and Methods

2.1. Material

Heat-inactivated fetal calf serum (FCS), sterile cell culture flasks and plates were obtained through Sterilab Services (Kempton Park, Johannesburg, South Africa). Dulbecco's minimum essential medium Eagle (D-MEM), penicillin, streptomycin and fungizone were purchased from Highveld Biological (Pty) Ltd. (Sandringham, SA). 2ME was supplied by Sigma-Aldrich (St. Louis, United States of America). An Annexin V-FITC Kit and an anti-cytochrome *c* FITC-conjugated antibody set were purchased from BIOCOM biotech (Pty) Ltd. (Clubview, South Africa). A fluorescein-FITC conjugated cyclin B1 antibody reagent set was purchased from The Scientific Group (Johannesburg, South Africa). Qiagen's Plant Mini Kit, PCR Clean-up kit, RNase-free DNase and Qiazol were purchased from Southern Cross Biotechnology (Pty) Ltd. (Cape Town, South Africa). The Nanodrop, an Axon Genepix 4000B Scanner and Agilent's SureHyb chambers at the African Centre of Gene Technology (ACGT) Microarray Facility (University of Pretoria, Pretoria, South Africa) were purchased from Inqaba Biotechnical Industries (Pty) Ltd. (Pretoria, SA), Molecular Devices Corporation, (Sunnyvale, California, United States of America) and Agilent Technologies (Pty) Ltd. (Palo Alto, California, United States of America) respectively. The fluorescence activated cell sorting (FACS) FC500 System flow cytometer equipped with an air-cooled argon laser excited at 488 nm was purchased from Beckman Coulter South Africa (Pty) Ltd. (Pretoria,

South Africa). Agilent's 44k 60-mer human oligo slides, Low RNA Input Fluorescent Linear Amplification Kit, 2x GEx Hybridization Buffer HI-RPM, Gene Expression (GE) Wash Buffer 1 and 2 and the Stabilization and Drying Solution were purchased from Agilent Technologies (Pty) Ltd. (Palo Alto, California, United States of America). All other chemicals were of analytical grade and were purchased from Sigma Chemical Co. (St. Louis, MO, USA).

2.2. Cell culture

The MCF-7 cell line (human breast epithelial carcinoma) was supplied by Highveld Biological (Pty) Ltd. (Sandringham, Johannesburg, South Africa). Cells were grown and maintained in 25 cm^2 tissue culture flasks in a humidified atmosphere at 37°C, 5% CO_2 in a Forma Scientific water-jacketed incubator (Ohio, United States of America). MCF-7 cells were cultured in DMEM and supplemented with 10% heat-inactivated FCS (56°C, 30 min), 100 U/ml penicillin G, 100 µg/ml streptomycin and fungizone (250 µg/l). A stock solution of 2 mM 2ME dissolved in dimethyl sulphoxide (DMSO) was prepared and diluted with medium to the desired concentrations prior to exposure of the cells. The medium of all control cells was supplemented with an equal concentration of DMSO (vehicle). The DMSO content of the final dilutions never exceeded 0.1% (v/v). A final concentration 1 µM 2ME was employed in all our studies, since Van Zijl *et al.* (2008) determined this to be the optimal concentration for the inhibition of growth in MCF-7 cells through dose-dependent investigations conducted in our laboratory [11]. Experiments were performed in either 6-well plates or 25 cm^2 cell culture flask. For six-well plates, exponentially growing cells were seeded at 250 000 cells per well in 3 ml maintenance medium in 6-well plates on heat-sterilized coverslips. After a 24 h incubation period at 37°C to allow for cell adherence, cells were exposed to 1µM 2ME and vehicle respectively and incubated for 24 h at 37°C. For 25 cm^2 cell culture flasks, exponentially growing MCF-7 cells were seeded at $1x10^6$ cells per 25 cm^2 flask to a final volume of 5 ml of maintenance medium. After 24 h attachment the medium was discarded and the cells were exposed to 1 µM 2ME (5 ml medium) and incubated for 24 h.

2.3. Flow cytometric quantification of cyclin B1 and cell cycle progression determination

A cyclin B1-fluorescein isothiocyanate (FITC) conjugated antibody was used in order to quantify cyclin B1 protein by employing flow cytometric analyses. After 24 h treatment in 25 cm^2 flasks, cells were trypsinized and fixated with 10 ml ice-cold 70% ethanol and stored at 4ºC for 24 h. After 24 h, the cells were trypsinized and washed with PBS. Cells ($1x10^6$) were incubated with either FITC-conjugated mouse immunoglobulin G (IgG) as a control or FITC-conjugated cyclin B1 for 30 min at room temperature. Cells were washed and resuspended in 0.5 ml PBS containing 40 µg/ml propidium iodide and 100 µg/ml RNase A for 30 min at 4°C.

FITC (FL1) and propidium iodide (FL3) fluorescence were measured with a FC500 System flow cytometer (Beckman Coulter South Africa (Pty) Ltd.) equipped with an air-cooled argon laser excited at 488nm. Data from at least 10 000 cells were analyzed with CXP software (Beckman Coulter South Africa (Pty) Ltd). Aggregated and aneuploid cells were removed from analysis by visual inspection. For cyclin B1 analyses, fluorescence of the FITC-conjugated isotypic control was normalized to 2% on an FL1-log vs FL3-lin dot-plot. Measurement of FITC-conjugated cyclin B1 fluorescence of control and exposed MCF-7 cells were measured utilizing the normalized area of the dot-plot. For cell cycle analyses, results are expressed as percentage of the cells in each phase. Cell cycle distributions from histograms generated by the CXP software were calculated with Multicycle (Phoenix Flow Systems, San Diego, CA).

2.4. Flow cytometric measurement of hydrogen peroxide and superoxide

Hydrogen peroxide (H_2O_2) generation was assessed using 2,7-dichlorofluorescein diacetate (DCFDA), a non-fluorescent probe, which upon oxidation by ROS and peroxides is converted to the highly fluorescent derivative DCF [21]. Superoxide generation was assessed using hydroethidine (HE). HE is oxidized by superoxide and not by hydroxyl radicals, singlet O_2, H_2O_2 or nitrogen radicals to a red fluorescing compound [22]. After 24 h exposure, cells were trypsinized, washed with PBS and $1x10^6$ cells were resuspended in 1 ml PBS. Cells were incubated with 20 μM DCFDA for 25 min and 10 μM HE for 15 min at 37°C. Hydrogen peroxide (20 μM) was added 5 min prior to measurement as a positive control for DCF formation. For DAF2-DA, 5 μM was added to the cells in PBS and incubated for 45 min at 37°C. DCF (FL1) and HE fluorescent product fluorescence (FL2) were measured with a FACS FC500 System flow cytometer equipped with an air-cooled argon laser excited at 488nm.

2.5. Morphology study – Fluorescent microscopy

A double fluorescent dye staining method was utilized in order to determine the effect that 2ME has on acidic vesicular organelle formation. Acridine orange is a lysosomotropic fluorescent compound that serves as a tracer for acidic vesicular organelles including autophagic vacuoles and lysosomes [23]. Cells undergoing autophagy will have an increased tendency for acridine orange staining when compared to viable cells. Hoechst 33342 is a fluorescent dye that can penetrate intact cell membranes of viable cells and cells undergoing apoptosis and stains the nucleus. After 24 h treatment in six well plates, 0.5 ml of Hoechst 33342 solution (3.5 μg/ml in PBS) was added to the medium to provide a final concentration of 0.9 μM and incubated for 30 min at 37°C in a CO_2 incubator. After 25 min, 0.5 ml of acridine orange solution (4 μg/ml) was added to the medium to provide a final concentration of 1

µg/ml and incubated for 5min at 37°C. Within 5 min the cover slips were mounted on microscope slides with mounting fluid (90% glycerol, 4% N-propyl-gallate, 6% PBS). The cells were examined with a Zeiss inverted Axiovert CFL40 microscope and Zeiss Axiovert MRm monochrome camera using Zeiss Filter 2 for Hoechst 33342 (blue emission) stained cells and Zeiss Filter 9 for acridine orange-stained (green emission) cells. In order to prevent fluorescent dye quenching, all procedures were performed in a dark room.

2.6. Morphology study – Transmission electron microscopy

Transmission electron microscopy (TEM) was used to determine the ultrastructure of intracellular components of exposed- and control cells. After 24 h treatment in 25 cm^2 flasks, cells were trypsinized, fixed in 2.5% glutaraldehyde in 0.075 M phosphate buffer (pH 7.4-7.6) and washed with 0.075 M phosphate buffer. Thereafter the cells were fixed in 0.25% aqueous osmium, dehydrated with increasing concentrations of ethanol (30%, 50%, 70%, 90%, 100%, 100%, 100%) and embedded in Quetol resin. Ultra-thin sections were prepared with a microtome and mounted on a copper grid. Samples were contrasted with 4% uranyl acetate and Reynolds' lead citrate. Samples were viewed with a Multi-purpose Philips 301 TEM at the Electron Microscopy unit of the University of Pretoria (Pretoria, South Africa).

2.7. Flow cytometric detection of Annexin V surface staining and propidium iodide permeability

Flow cytometric analyses were employed to measure indications of apoptosis. Annexin V was employed to measure the translocation of the membrane phospholipids, phosphatidylserine (PS), which is associated with apoptotic processes. Annexin V is a 35-36 kDa, Ca^{2+}-dependent, phospholipid binding protein with a high affinity for PS. After treatment in 25 cm^2 flasks, cells were trypsinized and $1x10^6$ cells were double-stained with Annexin V-FITC and propidium iodide according to the manufacturer's instructions (Miltenyi Biotec GmbH, Bergisch Gladbach, Germany). Propidium iodide (FL3) fluorescence and Annexin V (FL1) fluorescence were measured with a FACS FC500 System flow cytometer (Beckman Coulter South Africa (Pty) Ltd) equipped with an air-cooled argon laser excited at 488nm. Data from at least 30 000 cells were analyzed with CXP software (Beckman Coulter South Africa (Pty) Ltd.

2.8. Flow cytometric quantification of cytochrome c

An anti-cytochrome *c* FITC-conjugated antibody was employed to measure the mitochondrial-released intracellular cytochrome *c* levels. After 24 h of treatment in 25 cm^2 flasks, cells were trypsinized and $1x10^6$ cells were resuspended in 1 ml PBS. Cells were stained with FITC-conjugated mouse immunoglobulin G (IgG_1) as a control or FITC-conjugated cytochrome *c*. Staining was conducted according to the manufacturer's instructions (Assay Designs Inc, Michigan, USA). FITC (FL1) fluorescence was measured with a fluorescence activated cell sorting (FACS) FC500 System flow cytometer (Beckman Coulter South Africa (Pty) Ltd.) equipped with an air-cooled argon laser excited at 488 nm. Data from at least 10 000 cells were analyzed with CXP software (Beckman Coulter South Africa (Pty) Ltd). Fluorescence of the FITC-conjugated isotypic control was normalized to 1% for FL1-Log histograms and FITC-conjugated cytochrome *c* fluorescence of control- and exposed MCF-7 cells were plotted utilizing the normalized area of the histogram plot generated by the CXP software.

2.9. Microarray analysis of gene expression

Agilent's Human 1A Oligo 60-mer Microarray (V2) 44k slides were used to study expression changes induced by 24 h treatment of 2ME. A dye-swop methodology was employed whereby total RNA from vehicle-control and exposed cells from two biological replicates were combined per slide.

2.10. RNA extraction and integrity

Total RNA was isolated from vehicle-control and exposed MCF-7 cells using Qiagen's RNeasy with subsequent Qiazol purification. Cells were lysed with beta-mercaptoethanol containing guanidine isothiocyanate and the lysate was applied to QIAshredder spin columns and centrifuged for 2 min at 9000 x g. 1 ml Qiazol reagent was added to the flow-through and left for 5 min after which 0.3 ml chloroform was added. The sample was shaken vigorously and left at room temperature for 10 min. After 10 min the sample was centrifuged for 15 min at 4ºC at 12000 x g. The upper aqueous phase was removed and 1 volume 70% ethanol was added and gently mixed. This solution was divided into Qiagen Plant Mini Kit columns (700µl per column) and centrifuged for 15 s at 9000 x g. The flow-through was discarded and an on-column RNase-free DNase DNA digestion procedure to remove and DNA contaminants was followed as per the manufacturer's instructions. After washing the total RNA was quantified with a Nanodrop and tested for integrity by electrophoresis with a 1.5% agarose-formaldehyde gel. RNA was considered pure of organic

contamination (*e.g.* ethanol or phenol) with a 260/230 ratio greater than 1.5 and pure of protein contamination with a 260/280 ratio greater than 2. Only pure total RNA was used for cRNA synthesis. RNA was considered completely intact when clear 28S and 18S rRNA bands, with a 28S:18S intensity ratio was approximately 2:1.

2.11. Probe preparation, hybridization and microarray slide washing

Agilent's Low RNA Input Fluorescent Linear Amplification Kit was used to generate fluorescently labeled cRNA. Briefly, 5 µg total RNA from exposed and control-exposed RNA samples were used for amplification into double stranded DNA ulitizing an MMLV-Reverse transcriptase and dT-T7 primer. Labeled cRNA was produced using the T7 polymerase and washed using Qiagen's RNeasy Mini kits. 825 ng cRNA was fragmented for 30 min at 60˚C and subsequently hybridized to Agilent Human 1A (V2) oligonucleotide 44K microarray slides according to the manufactures guidelines using Agilent's 2x GEx Hybridization Buffer HI-RPM in Agilent's SureHyb chambers. Hybridization was carried out over 17 h in the dark in a rotating hybridization chamber set at 65˚C and 10 rpm. Slides were washed using Agilent's Gene Expression Wash Buffer and Stabilization and Drying Solution according to recommendations. The slides were disassembled in Agilent's Gene Expression (GE) Wash Buffer 1 and washed for 1 min at room temperature. The slides were transferred to GE Wash Buffer 2 at elevated temperature (37˚C) and washed for 1 min and then transferred to pure acetonitrile for 10 s. The slides were then transferred to Stabilization and Drying Solution for 30 s after which it was scanned immediately after careful removal from the solution.

2.12. Scanning and data analysis - Microarray

Slides were scanned with the Axon Genepix 4000B Scanner (Molecular Devices Corporation, Sunnyvale, CA, USA) provided by the African Centre of Gene Technology (ACGT) Microarray Facility at the University of Pretoria, Pretoria, South Africa. Spotfinding was performed using Genepix Pro 6.1 (Molecular Devices Corporation, Sunnyvale, CA, USA). Saturated spots, spots with an uneven background, non-uniform spots and spots with a low intensity *vs.* background ratio were removed from further analysis by excluding the spots that satisfied the following parameters. The following features were flagged as "Bad" and were removed from further analysis using Genepix 6.1 software:

Saturated spots: [F532 % Sat.] > 30 And [Ratio of Means (635/532)] > 0.75 Or [F635 % Sat.] > 30 And [Ratio of Means (635/532)] < 1.3333

Spots with an uneven background: ([B635 Mean] > (1.5*[B635 Median]) Or [B532 Mean] > (1.5*[B532 Median])) And ([B635 Median] > 40 Or [B532 Median] > 40)

Non-uniform spots: [Ratio of Medians (635/532)] > (4.0*[Rgn Ratio (635/532)]) Or [Ratio of Medians (635/532)] < (0.25*[Rgn Ratio (635/532)])

Low intensity *vs.* background ratio: [% > B635+2SD] < 10 Or [% > B532+2SD] < 10

Statistical analysis after spotfinding was conducted using Limma with the LimmaGUI interface [24-25]. Background correction was done with the normal+exponential (Normexp) convolution model with an offset value set to 50 [26-27]. Genepix Flag weightings that were flagged as "Bad" were excluded from further analysis. Normalization within arrays was performed with the Global Loess method and Aquantile normalization between arrays was performed in order to normalize expression intensities so that the intensities and log-ratios have similar distributions across a series of arrays [27]. The Least squares linear model fit method was employed and the *P*-values were adjusted for multiple testing utilizing the Benjamini and Hochberg's step-up method for controlling the false discovery rate [28]. Genes that had a *B*-value of greater than zero were considered statistically significantly differentially expressed. The *B*-statistic is defined as log-odds that that gene is differentially expressed and a *B*-statistic of zero corresponds to a 50/50 chance that the gene is differentially expressed [27]. The gene names acquired from the gene expression list of genes considered differentially expressed were converted to Entrez Gene IDs utilizing the DAVID Gene ID Conversion Tool [29]. Biologic interpretation and functional analysis of the converted gene lists were performed by mapping differentially expressed genes to biochemical pathways and Gene Ontology (GO) categories using Gene Annotation Co-occurrence Discovery (GENECODIS) [30]. Graphical biochemical pathways were designed with CellDesigner 3.5.1 [31].

2.13. Statistical analysis of data

Data obtained from three independent experiments (each conducted in six replicates) are shown as the mean ±SD and were statistically analyzed for significance using the analysis of variance (ANOVA)-single factor model followed by a two-tailed Student's *t*-test. Means are presented in bar charts, with T-bars referring to standard deviations. *P*-values < 0.05 were regarded as statistically significant and indicated by an asterisk (*). Measurement of FITC-and DCF-derived fluorescence was expressed as a percentage of the value measured for vehicle-treated exposed cells (relative fluorescence).

3. Results

3.1. Flow cytometric quantification of cyclin B1 and cell cycle progression determination

Intracellular cyclin B1 levels were evaluated by means of flow cytometric analyses. Cyclin B1 levels were increased in 2ME-treated cells during the G_2/M phase when compared to the vehicle-treated control (Figures 1 and 2). An increase to 38±7% was observed in 2ME-treated cells when compared to vehicle-treated control cells (16±3.7%) (Figure 2). DNA content analyses by means of flow cytometry showed a statistically significant increase in the G_2/M phase in 2ME-treated cells (23.07±1.7%) compared to vehicle-treated cells (19.3±0.9%) (Figures 3 and 4). Vehicle-treated cells also showed a marked increase in S-phase (61.7±4.1%) when compared to 2ME-treated cells (32.6±5.5%), while 2ME-treated showed a marked increase in the sub-G_1 population (14.8±1.2%) when compared to the vehicle-treated cells (0.98±0.3%) (Figures 3 and 4). These results suggest that 2ME-treated cells in the G_2/M phase enter stages of apoptosis (sub-G_1); rather than completing mitosis, entering G_1-phase and subsequently entering the S-phase.

3.2. Flow cytometric measurement of hydrogen peroxide and superoxide

In order to investigate the extent of hydrogen peroxide and superoxide production in 2ME-treated cells compared to vehicle-treated, flow cytometric analyses of MCF-7 cells loaded with the H_2O_2-sensitive the fluorophore DCFDA and the superoxide sensitive probe HE were conducted. Figure 5A shows an increase in mean fluorescence intensity of DCF in 2ME-treated cells when compared to vehicle-treated cells. Statistical analyses indicate a 1.54±0.17-fold increase over the vehicle-treated control, while the 20 μM H_2O_2-treated positive control indicated a 1.92±0.33-fold increase in mean fluorescence intensity when compared to the vehicle-treated control (Figure 5B). These results indicate that 2ME induces H_2O_2 formation in MCF-7 cells. No significant differences in superoxide levels between 2ME-treated and vehicle-treated control cells were observed ($P = 0.36$) (Figures 6A and 6B).

3.3. Morphology study – Fluorescent microscopy

Hoechst 33342 staining of 1 μM 2ME-treated revealed an increase in cells in metaphase, as well as an increase in the amount of cells in tripolar metaphase when compared to the vehicle-treated control (Figure 7A and 7B). Apoptotic body formation was not as prominent in 2ME-treated cells (data not shown) when compared to Actinomycin D-treated cells (Figure 7C). Acridine orange was

used as a lysosomotropic tracer for acidic vesicular organelles including autophagic vacuoles and lysosomes [23]. Cells undergoing autophagy will have an increased tendency for acridine orange staining when compared to viable cells. Qualitative analyses of 1 μM 2ME-treated showed an increase in acridine orange staining when compared to the vehicle-treated controls cells (Figure 8A and 8B). The increased staining effect was more pronounced in cells that were in metaphase block (Figure 7B and 8B). Actinomycin D-treated (0.2 μg/ml) cells in late stages of apoptosis showed a decrease in staining with acridine orange (Figure 8C).

3.4. Morphology study – Transmission electron microscopy

An increase in the formation of vacuoles in 2ME-treated cells was observed by means of transmission electron microscopy when compared to vehicle-treated cells (Figure 9A and 9B). This suggests, although not conclusively, an increase in autophagic activity as revealed above by acridine orange staining. Hypercondensed chromatin was observed in Actinomycin D-treated cells, indicating late stages of apoptosis (Figure 9C).

3.5. Flow cytometric detection of Annexin V surface staining and propidium iodide permeability

Quantitative analyses of the externalization of the membrane phosphatidylserine with Annexin V were determined in order to detect early and late apoptotic processes. Propidium iodide measured the amount of necrotic cells. 2ME-treated cells showed an increase in early and late stages of apoptosis when compared to the vehicle-treated cells. (Figures 10A-B). 2ME-treated cells revealed 11.14% cells to be present in early apoptosis and 3.95% of cells were in late stages of apoptosis (Table 1).

3.6. Flow cytometric quantification of cytochrome c

Fluorochromatic quantification of FITC-conjugated cytochrome *c* antibodies in MCF-7 cells was conducted by means of flow cytometry analyses. Figure 11B shows a slight increase in FITC-conjugated cytochrome *c* in 2ME-treated cells when compared to the vehicle-treated control (Figure 11A-B). Statistical analyses indicated a significant 1.16±0.08-fold increase in FITC-conjugated cytochrome *c* in 2ME-treated cells over the vehicle-treated control (normalized to 1) (Figure 12). These results indicate that mitochondrial release of cytochrome *c* is slightly increased in 2ME-treated MCF-7 cells.

3.7. Gene expression - Microarray

Agilent's Human 1A Oligonucleotide Microarray slides with more than 41 000 60-mer oligonucleotide human genes and transcripts were employed to collect genomic information on the mechanism of action of 2ME in MCF-7 cells. Spotfinding was conducted with Genepix Pro 6.1. Genes that were considered statistically significantly differentially expressed (*B*-value > 0) and upregulated or downregulated in 2ME-treated cells are summarized in Tables 2 and 3 respectively. 775 genes out of the 41 000 (1.89%) transcripts were included for further analyses. Mapping of differentially expressed genes to biochemical pathways and GO categories was performed using GENECODIS. The statistically significant differentially expressed genes ($B > 0$) were mapped to regulation of transcription, signal transduction, cell cycle, apoptosis, nucleosome assembly, reactive oxygen species metabolism, DNA repair, microtubule base movement, cell adhesion and ribosomal activity (Supplementary Tables 1 and 2).

4. Discussion

In the present study we have demonstrated the effects of 1 μM 2ME in MCF-7 cells after 24 h of exposure. 2ME treatment resulted in increased levels of cyclin B1. Similar results were obtained by Bhati *et al*. (2007) in MDA-MB-435 breast cells and Attalla *et al.* (1996) in Jurkat cells [6, 32]. Expression of genes associated with microtubule dynamics were affected in 2ME-treated cells. Kamath *et al*. (2006) demonstrated that suppression of microtubule dynamics (and not microtubule depolymerization) plays a key role in mitosis in 2ME-treated MCF-7 cells [9]. In the present study several genes involved in microtubule dynamics were downregulated in 2ME-treated cells. These genes include BUB3, SPC25, ASPM, CENPE, CENPJ, CENPT, CEP55, as well as tubulin alpha- and beta genes, while SPIN2B was upregulated. BUB3 is required for the establishment of efficient kinetochore-microtubule attachments before the completion of mitosis. SPC25 plays a role in proper execution of mitotic events associated with kinetochore components and ASPM promotes spindle organization [33-35]. CENPE is a motor protein that carries chromosomes toward the metaphase plate and contributes to the capture and stabilization of spindle microtubules by kinetochores [36]. CENPJ (CPAP) is responsible for maintaining centrosome integrity and normal spindle morphology during cell division [37]. Relatively little is known about the function of CENPT, CEP55 and SPIN2B genes, however, overexpression of SPIN1 has been implicated in induced cell cycle delay in metaphase and mitotic spindle defects [38].

Bhati *et al*. (2007) demonstrated that the APC is inhibited in response to 2 μM 2ME in MDA-MB-435 breast cells [6]. They further demonstrated that genes involved in mitotic checkpoint complex (MCC) signaling (including NIMA, Bub1, Mad2) were

upregulated and that APC activity might be inhibited as a result of increased MCC signaling [6]. The MCC ensures accurate segregation of mitotic chromosomes by delaying anaphase onset until each kinetochore has properly attached to the mitotic spindle [39]. The MCC is activated in response to mitotic microtubules unattached to kinetochores and the system converges to inhibit the activity of the anaphase promoting complex/cyclosome-cell division cycle 20 (APC/C-cdc20) complex [39-42]. Activated APC/C-cdc20 targets cyclin B1 for ubiquitination and allows for a cell to transit from metaphase to anaphase [43]. Increased levels of cyclin B1 observed in the present study can in part be explained by decreased activity of the APC/C-cdc20 complex induced by 2ME; possibly through MCC activation and downregulation of cdc20 expression. This would lead to decreased degradation of the cyclin B1 protein and an increase in intracellular cyclin B1 evident in the present study. The observations of decreased mRNA expression of cyclins B1 and B2, as well as cdc2 are consistent with the findings of Zoubine *et al*. (1999) who revealed a decrease in the expression of cdc2 and cyclin B1 genes in 1 μM 2ME-treated MCF-7 cells [10]. While cdc2 mRNA expression was decreased in 2ME-treated MCF-7 cells, van Zijl *et al*. (2008) and Attalla *et al.* (1996) showed that cdc2 activity was significantly increased in 1 μM 2ME-treated MCF-7 and Jurkat cells respectively [11, 32]. Increased cdc2 activity can be explained by increased levels of cyclin B1 since cdc2 requires intact cyclin B1 protein.

Cell cycle analyses revealed an increase in cells in the G_2/M phase, as well as in the number of cells present in the sub-G_1 phase. These results are consistent with the findings of experiments in other cell lines that indicated an accumulation of cells in the G_2/M-phase in 2ME-treated cells [6, 44-46]. Active cyclin B1-cdc2 levels needed for mitotic entry are lower than active cyclin B1-cdc2 levels needed for mitotic progression [47]. The findings that 2ME treatment of MCF-7 leads to a decrease in cdc2 and cyclin B1 expression, but an increase in cyclin B1 protein levels and cdc2 activity further explains the mitotic block. A sufficient amount of cyclin B1-cdc2 may be enough for mitotic entry, but too low (as a result of decreased cdc2 and cyclin B1 expression) for mitotic progression in 2ME-treated cells [32]. Cdc2 regulates the activity of the APC/C-Cadherin 1 (APC/C-cdh1) complex through phosphorylation and subsequent prevention of APC/C association of cdh. The APC/C-cdh1 complex is responsible for the targeted degradation of securin and subsequent release of separase, which is responsible for cohesin cleavage to allow for sister chromatid separation and the onset of anaphase [48]. Elevated activity of cdc2 activity would thus abrogate the activity of the APC/C-cdh1 complex, resulting in cells in a G_2/M arrest, as well as cells blocked in metaphase.

A marked decrease of cells in S-phase was also observed in 2ME-treated cells. A number of intra-S phase related checkpoint proteins involved in DNA repair were downregulated in 2ME-treated cells [49]. Genes of interest that play a role in DNA repair that were downregulated in 2ME-treated MCF-7 cells include ATR, BRCA1, DDB1, PARP1 and TOPBP1. Genes of proteins

constituting parts of the replisome (PCNA, RFC1 and RFC4) were also downregulated. Data obtained from gene expression analysis together with observations of an increase in the sub-G_1 fraction and a decrease in the number of cells in the S-phase indicates that 2ME-treated cells are likely not to re-enter mitosis.

Generation of superoxide has previously been associated with 2ME treatment. Gao *et al.* (2005) observed an increase in superoxide generation in 4 μM 2ME-treated U937 human leukemia cells after 6 h treatment [50]. She *et al.* (2007) also observed an increase in superoxide levels in 2 μM 2ME-treated human myeloid leukemia HL-60 and U937 cells [51]. Chen *et al.* (2008) used a 0.1 mM 2ME concentration to induce superoxide generation in transformed HEK293, U87 and HeLa cancer cell lines [52]. Destruction of superoxide is catalyzed by manganese superoxide dismutase within the mitochondrial matrix and intracellular superoxide is destroyed by copper-zinc superoxide dismutase [53]. Kachadourian *et al.* demonstrated that 2ME (0.1 mM) does not inhibit superoxide dismutase and proposed the formation of estrogen semiquinone radicals with subsequent formation of superoxide [54-55]. The present study focused on a lower concentration of 2ME (1 μM) and no significant difference in superoxide levels between vehicle-treated and 2ME-treated cells was detected.

Generation of H_2O_2 as a result of 2ME treatment has been implicated as a mediator of apoptosis induction. H_2O_2 forms part of signal transduction pathways including the ERK, JNK and p38 pathways [56]. Fukui and Zhu (2009) demonstrated that 1.5-2 μM 2ME treatment of MDA-MB-435 breast cells induced activation of ERK, JNK and p38 proteins [13]. In Ewing sarcoma cells, 2ME-treated cells showed an increase in the formation of H_2O_2 and rapid induction of the JNK pathway. This resulted in decreased mitochrondrial membrane potential, release of cytochrome *c* and downstream activation of caspases [57]. The present study demonstrated an increase in H_2O_2 generation in MCF-7 cells in response to 2ME treatment, as well as an increase in intracellular levels of cytochome *c*. One possible source of H_2O_2 is the inactivation of peroxiredoxin 1 (Prx 1). Prx 1 reduces H_20_2 to water and oxygen, and during mitosis actives cdc2 responsible for the phosphorylation and inactivation of the PRx 1 enzyme [58]. Thus, prolonged cdc2 activity during metaphase and subsequent elevation of H_20_2 may be due to PRx 1 inhibition. Another interesting finding is the upregulation of spermine oxidase (SMOX). SMOX is the only catabolic enzyme that is able to specifically oxidise spermine the spermidine [59-60]. The reaction results in the formation of H_2O_2 [60]. In human breast cancer cells as well as mouse neuroblastoma cells, SMOX overexpression results in an antiproliferative effect as a result of oxidative stress [61-62]. Overexpression of SMOX as a result of 2ME treatment is thus another possible source of H_2O_2. Differentially expressed genes associated with ROS-signaling include the upregulation of mitogen-activated protein kinase 4 (MKK4) and mitogen-activated

protein kinase 6 (MKK6). Heme oxygenase-1 (HO-1) was also upregulated in 2ME-treated MCF-7 cells and it is well known that HO-1 mRNA is strongly induced by H_2O_2 and ferric iron [63-65].

H_2O_2 and other ROS are known to activate several growth inhibitory pathways such as authophagy. Activation of autophagic processes is regulated through inactivation of mammalian target of rapamycin (mTOR) and Beclin 1. Active mTOR inhibits LC3 activity which is required for the formation process of autophagosomes [66]. In U937 leukemia cells, 4 μM 2ME gradually decreased mTOR and phospho-mTOR protein levels over time and catalase prevented this gradual decrease [50]. It was argued that H_2O_2, as well as superoxide formation are primarily responsible for these signaling events in U937 leukemia cells [50]. Recently it has been demonstrated that H_2O_2 and other ROS can induce autophagic processes through inhibition of the autophagy-related gene 4 (Atg4) as well as induction of Beclin 1 expression [67]. Chen *et al*. (2008) demonstrated that autophagic processes were induced in the HEK293 transformed cell line and the cancer cell lines U87 and HeLa [52]. They further demonstrated that these processes are caused as a result of H_2O_2 formation. In the present study, we have demonstrated an increase in acridine orange staining in 2ME-treated MCF-7 cells, as well as an increase in the formation of vacuoles. Increased acridine orange staining in cells is an indication of increased acidic vesicle formation and these are associated with increased lysosomal and/or autophagic processes [23]. Furthermore, gene expression analysis revealed the downregulation of eukaryotic translation initiation factors (EIFs) involved in mRNA translation and are controlled downstream of mTOR activity [66]. These include EIF4E, EIF4A2, EIF4B, EIF2C1 and EIF3S6. Several genes associated with ribosomal activity were also downregulated. Similar results were obtained by Bhati *et al.* (2007) where a decrease in the expression of ribosomal proteins and inhibition of protein translation was observed in 2ME-treated MDA-MB-435 cells [6]. Also, phosphatidylinositol-3,4,5-trisphosphate 3-phosphatase and dual-specificity protein phosphatase (PTEN) was slightly up-regulated in response to 2ME-treatment. PTEN overexpression is able to inhibit mTOR activity through the phosphoinositide 3-kinase/ protein kinase B/ tuberous sclerosis complex 2 (PI3K/Akt/TSC2) pathway [68]. mTOR inhibition plays a role in HIF-1a activity by preventing HIF-1a transcriptional activation and this in turn plays a role in the antiangiogenic effects of mTOR inhibitors [69-70]. Our results together with related findings from other studies suggest that autophagic processes are also activated in 2ME-treated MCF-7 cells through an mTOR-mediated pathway whereby ROS and PTEN overexpression are likely to play a role in abrogating the activity of mTOR.

Induction of apoptosis has been associated with 2ME treatment in various cell lines. JNK signaling and subsequent phosphorylation and inactivation of anti-apoptotic Bcl-2 proteins is a common mechanism of activating the intrinsic apoptosis pathway [13, 50, 57]. Early and late stages of apoptosis induction were observed in 2ME-treated MCF-7 cells. A slight increase in intracellular

cytochrome *c* formation was also demonstrated in 2ME-treated cells which indirectly indicate an increase in mitochondrial permeabilization, possibly due to inactivation of the anti-apoptotic Bcl-2 protein. Tumor necrosis factor (ligand) superfamily, member 10 (TNFSF10/TRAIL) was also found to be upregulated. Upregulation of TNFSF10/TRAIL can in part explain the up-regulation of death receptor 5 in 2ME-treated breast carcinoma cells MDA-MB-231 and MDA-MB-435, cervical carcinoma cells HeLa, prostate carcinoma cells PC-3, and glioma cells U87-MG cells [14]. MCF-7 cells, however, are deficient in caspase-3 expression and undergo apoptosis without showing inter-nucleosomal cleavages [71]. It is thus unlikely that cytochrome *c* release plays a significant role in apoptosis induction through caspase activation in MCF-7 cells. Gene expression analyses revealed the upregulation of proapototic genes including BCL2 binding component 3, TP53INP1 tumor protein p53 inducible nuclear protein 1, cyclin-dependent kinase inhibitor 2A and calpastatin (CAST). *v*-Myc myelocytomatosis viral oncogene homolog (avian) (MYC) was found to be downregulated in 2ME-treated MCF-7 cells. The present study also revealed the downregulation of genes associated with nucleosome assembly, as well as cell adhesion.

From the data and presently available literature, it is thus proposed that interference with microtubule dynamics and subsequent activation of the MCC cause inhibition of cyclin B ubiquination and degradation, leading to increased cdc2 activity, a metaphase block and inactivation of PRx1 (Figure 13). Increased formation of ROS play a role in pro-apoptotic ROS signaling which results in the activation of growth inhibitory pathways including apoptosis and autophagy. In conclusion, 2ME treatment of MCF-7 cells resulted in increased cyclin B1 protein levels, cell cycle arrest, increased H_2O_2 formation, increased intracellular levels of cytochome *c* and vacuole formation together with increased acidic vesicle formation. Gene expression analysis revealed that 2ME interferes with microtubule dynamics, mitotic checkpoint signaling, cyclin B1 degradation, cdc2 activity and pro-apoptotic events. Furthermore, microarray gene expression analysis showed a decreased expression of genes involved in mRNA translation and autophagy-related processes, including ribosomal proteins and EIFs. Thus, a novel finding namely the induction of both apoptosis and autophagy as a possible combination of types of cell death induced by 2ME in MCF-7 cells is suggested and therefore the present study contributes to the mechanism of its action.

Acknowledgements

This research was supported by grants from the Medical Research Council of South Africa (AG374, AK076), the Cancer Association of South Africa (AK246) and the Struwig-Germeshuysen Cancer Research Trust of South Africa (AJ038). Electron microscopy was conducted at the Electron microscopy Unit at the University of Pretoria and flow cytometric analyses were performed at the Department of Pharmacology at the Faculty of Health Sciences (University of Pretoria). Microarray data analysis

facilities were provided by the African Centre of Gene Technology (ACGT) Microarray Facility (University of Pretoria, Pretoria, South Africa) and the Bioinformatics and Computational Biology Unit (University of Pretoria, Pretoria, South Africa).

References

1. S.L. Mooberry, Mechanism of action of 2-methoxyestradiol: new developments, Drug Resist Updat 6(6) (2003) 355-361.

2. S.P. Newman, C.R. Ireson, H.J. Tutill, J.M. Day, M.F. Parsons, M.P. Leese, B.V. Potter, M.J. Reed, A. Purohit, The role of 17beta-hydroxysteroid dehydrogenases in modulating the activity of 2-methoxyestradiol in breast cancer cells, Cancer Res 66(1) (2006) 324-330.

3. D. Matei, J. Schilder, G. Sutton, S. Perkins, T. Breen, C. Quon, C. Sidor, Activity of 2 methoxyestradiol (Panzem NCD) in advanced, platinum-resistant ovarian cancer and primary peritoneal carcinomatosis: a Hoosier Oncology Group trial, Gynecol Oncol 115(1) (2009) 90-96.

4. W.E. Fogler, K.M. Volker, G.M. Swartz, S.M. Plum, S.J. Strawn, T.M. LaVallee, C.F. Sidor, A.M. Treston, The Antitumor Activity of 2-Methoxyestradiol is Maximized by Maintaining a Threshold Concentration Over a 24-Hour Dosing Interval, Proceedings of the AACR-NCIEORTC International Conference on Molecular Targets and Cancer Therapeutics, 2005. pp. 173, B180.

5. A.J. Tevaarwerk, K.D. Holen, D.B. Alberti, C. Sidor, J. Arnott, C. Quon, G. Wilding, G. Liu, Phase I trial of 2-methoxyestradiol NanoCrystal dispersion in advanced solid malignancies, Clin Cancer Res 15(4) (2009) 1460-1465.

6. R. Bhati, Y. Gokmen-Polar, G.W. Sledge, Jr., C. Fan, H. Nakshatri, D. Ketelsen, C.H. Borchers, M.J. Dial, C. Patterson, N. Klauber-DeMore, 2-methoxyestradiol inhibits the anaphase-promoting complex and protein translation in human breast cancer cells, Cancer Res 67(2) (2007) 702-708.

7. R.K. Dubey, E.K. Jackson, Potential vascular actions of 2-methoxyestradiol, Trends Endocrinol Metab 20(8) (2009) 374-379.

8. N.J. Mabjeesh, D. Escuin, T.M. LaVallee, V.S. Pribluda, G.M. Swartz, M.S. Johnson, M.T. Willard, H. Zhong, J.W. Simons, P. Giannakakou, 2ME2 inhibits tumor growth and angiogenesis by disrupting microtubules and dysregulating HIF, Cancer Cell 3(4) (2003) 363-375.

9. K. Kamath, T. Okouneva, G. Larson, D. Panda, L. Wilson, M.A. Jordan, 2-Methoxyestradiol suppresses microtubule dynamics and arrests mitosis without depolymerizing microtubules, Mol Cancer Ther 5(9) (2006) 2225-2233.

10. M.N. Zoubine, A.P. Weston, D.C. Johnson, D.R. Campbell, S.K. Banerjee, 2-methoxyestradiol-induced growth suppression and lethality in estrogen-responsive MCF-7 cells may be mediated by down regulation of p34cdc2 and cyclin B1 expression, Int J Oncol 15(4) (1999) 639-646.

11. C. Van Zijl, M.L. Lottering, F. Steffens, A. Joubert, In vitro effects of 2-methoxyestradiol on MCF-12A and MCF-7 cell growth, morphology and mitotic spindle formation, Cell Biochem Funct 26(5) (2008) 632-642.

12. J.S. Lewis, T.J. Thomas, R.G. Pestell, C. Albanese, M.A. Gallo, T. Thomas, Differential effects of 16alpha-hydroxyestrone and 2-methoxyestradiol on cyclin D1 involving the transcription factor ATF-2 in MCF-7 breast cancer cells, J Mol Endocrinol 34(1) (2005) 91-105.

13. M. Fukui, B.T. Zhu, Mechanism of 2-methoxyestradiol-induced apoptosis and growth arrest in human breast cancer cells, Mol Carcinog 48(1) (2009) 66-78.

14. T.M. LaVallee, X.H. Zhan, M.S. Johnson, C.J. Herbstritt, G. Swartz, M.S. Williams, W.A. Hembrough, S.J. Green, V.S. Pribluda, 2-methoxyestradiol up-regulates death receptor 5 and induces apoptosis through activation of the extrinsic pathway, Cancer Res 63(2) (2003) 468-475.

15. J.M. Rae, C.J. Creighton, J.M. Meck, B.R. Haddad, M.D. Johnson, MDA-MB-435 cells are derived from M14 melanoma cells--a loss for breast cancer, but a boon for melanoma research, Breast Cancer Res Treat 104(1) (2007) 13-19.

16. A. Joubert, C. Maritz, F. Joubert, Bax/Bcl-2 expression levels of 2-methoxyestradiol-exposed esophageal cancer cells, Biomed Res 26(3) (2005) 131-134.

17. A. Joubert, C. Maritz, F. Joubert, Influence of prostaglandin A2 and 2-methoxyestradiol on Bax and Bcl-2 expression levels in cervical carcinoma cells, Biomed Res 26(2) (2005) 87-90.

18. S.Z. Bu, Q. Huang, Y.M. Jiang, H.B. Min, Y. Hou, Z.Y. Guo, J.F. Wei, J.W. Wang, X. Ni, S.S. Zheng, p38 Mitogen-activated protein kinases is required for counteraction of 2-methoxyestradiol to estradiol-stimulated cell proliferation and induction of apoptosis in ovarian carcinoma cells via phosphorylation Bcl-2, Apoptosis 11(3) (2006) 413-425.

19. S. Bu, A. Blaukat, X. Fu, N.E. Heldin, M. Landstrom, Mechanisms for 2-methoxyestradiol-induced apoptosis of prostate cancer cells, FEBS Lett 531(2) (2002) 141-151.

20. R.U. Janicke, M.L. Sprengart, M.R. Wati, A.G. Porter, Caspase-3 is required for DNA fragmentation and morphological changes associated with apoptosis, J Biol Chem 273(16) (1998) 9357-9360.

21. G. Rothe, G. Valet, Flow cytometric analysis of respiratory burst activity in phagocytes with hydroethidine and 2',7'-dichlorofluorescin, J Leukoc Biol 47(5) (1990) 440-448.

22. H. Zhao, S. Kalivendi, H. Zhang, J. Joseph, K. Nithipatikom, J. Vasquez-Vivar, B. Kalyanaraman, Superoxide reacts with hydroethidine but forms a fluorescent product that is distinctly different from ethidium: potential implications in intracellular fluorescence detection of superoxide, Free Radic Biol Med 34(11) (2003) 1359-1368.

23. D.J. Klionsky, A.M. Cuervo, P.O. Seglen, Methods for monitoring autophagy from yeast to human, Autophagy 3(3) (2007) 181-206.

24. G.K. Smyth, Linear models and empirical bayes methods for assessing differential expression in microarray experiments, Stat Appl Genet Mol Biol 3 (2004) Article3.

25. J.M. Wettenhall, G.K. Smyth, limmaGUI: a graphical user interface for linear modeling of microarray data, Bioinformatics 20(18) (2004) 3705-3706.

26. M.E. Ritchie, J. Silver, A. Oshlack, M. Holmes, D. Diyagama, A. Holloway, G.K. Smyth, A comparison of background correction methods for two-colour microarrays, Bioinformatics 23(20) (2007) 2700-2707.

27. G.K. Smyth, T. Speed, Normalization of cDNA microarray data, Methods 31(4) (2003) 265-273.

28. Y. Benjamini, Y. Hochberg, Controlling the False Discovery Rate: A Practical and Powerful Approach to Multiple Testing, Journal of the Royal Statistical Society. Series B (Methodological) 57(1) (1995) 289-300.

29. W. Huang da, B.T. Sherman, R.A. Lempicki, Systematic and integrative analysis of large gene lists using DAVID bioinformatics resources, Nat Protoc 4(1) (2009) 44-57.

30. P. Carmona-Saez, M. Chagoyen, F. Tirado, J.M. Carazo, A. Pascual-Montano, GENECODIS: a web-based tool for finding significant concurrent annotations in gene lists, Genome Biol 8(1) (2007) R3.

31. A. Funahashi, M. Morohashi, H. Kitano, N. Tanimura, CellDesigner: a process diagram editor for gene-regulatory and biochemical networks BIOSILICO 1(5) (2003) 159-162.

32. H. Attalla, T.P. Makela, H. Adlercreutz, L.C. Andersson, 2-Methoxyestradiol arrests cells in mitosis without depolymerizing tubulin, Biochem Biophys Res Commun 228(2) (1996) 467-473.

33. E. Logarinho, T. Resende, C. Torres, H. Bousbaa, The human spindle assembly checkpoint protein Bub3 is required for the establishment of efficient kinetochore-microtubule attachments, Mol Biol Cell 19(4) (2008) 1798-1813.

34. R. Bharadwaj, W. Qi, H. Yu, Identification of two novel components of the human NDC80 kinetochore complex, J Biol Chem 279(13) (2004) 13076-13085.

35. M. van der Voet, C.W. Berends, A. Perreault, T. Nguyen-Ngoc, P. Gonczy, M. Vidal, M. Boxem, S. van den Heuvel, NuMA-related LIN-5, ASPM-1, calmodulin and dynein promote meiotic spindle rotation independently of cortical LIN-5/GPR/Galpha, Nat Cell Biol 11(3) (2009) 269-277.

36. H. Yardimci, M. van Duffelen, Y. Mao, S.S. Rosenfeld, P.R. Selvin, The mitotic kinesin CENP-E is a processive transport motor, Proc Natl Acad Sci U S A 105(16) (2008) 6016-6021.

37. J.H. Cho, C.J. Chang, C.Y. Chen, T.K. Tang, Depletion of CPAP by RNAi disrupts centrosome integrity and induces multipolar spindles, Biochem Biophys Res Commun 339(3) (2006) 742-747.

38. P. Zhang, B. Cong, H. Yuan, L. Chen, Y. Lv, C. Bai, X. Nan, S. Shi, W. Yue, X. Pei, Overexpression of spindlin1 induces metaphase arrest and chromosomal instability, J Cell Physiol 217(2) (2008) 400-408.

39. D.J. Lew, D.J. Burke, The spindle assembly and spindle position checkpoints, Annu Rev Genet 37 (2003) 251-282.

40. D.J. Baker, M.M. Dawlaty, P. Galardy, J.M. van Deursen, Mitotic regulation of the anaphase-promoting complex, Cell Mol Life Sci 64(5) (2007) 589-600.

41. H. Yu, Regulation of APC-Cdc20 by the spindle checkpoint, Curr Opin Cell Biol 14(6) (2002) 706-714.

42. J.M. Peters, The anaphase promoting complex/cyclosome: a machine designed to destroy, Nat Rev Mol Cell Biol 7(9) (2006) 644-656.

43. E.R. Kramer, N. Scheuringer, A.V. Podtelejnikov, M. Mann, J.M. Peters, Mitotic regulation of the APC activator proteins CDC20 and CDH1, Mol Biol Cell 11(5) (2000) 1555-1569.

44. N.N. Zhou, X.F. Zhu, J.M. Zhou, M.Z. Li, X.S. Zhang, P. Huang, W.Q. Jiang, 2-Methoxyestradiol induces cell cycle arrest and apoptosis of nasopharyngeal carcinoma cells, Acta Pharmacol Sin 25(11) (2004) 1515-1520.

45. A. Lis, M.J. Ciesielski, T.A. Barone, B.E. Scott, R.A. Fenstermaker, R.J. Plunkett, 2-Methoxyestradiol inhibits proliferation of normal and neoplastic glial cells, and induces cell death, in vitro, Cancer Lett 213(1) (2004) 57-65.

46. L. Li, S. Bu, T. Backstrom, M. Landstrom, U. Ulmsten, X. Fu, Induction of apoptosis and G2/M arrest by 2-methoxyestradiol in human cervical cancer HeLaS3 cells, Anticancer Res 24(2B) (2004) 873-880.

47. A. Lindqvist, W. van Zon, C. Karlsson Rosenthal, R.M. Wolthuis, Cyclin B1-Cdk1 activation continues after centrosome separation to control mitotic progression, PLoS Biol 5(5) (2007) e123.

48. F. Uhlmann, F. Lottspeich, K. Nasmyth, Sister-chromatid separation at anaphase onset is promoted by cleavage of the cohesin subunit Scc1, Nature 400(6739) (1999) 37-42.

49. A. Sancar, L.A. Lindsey-Boltz, K. Unsal-Kacmaz, S. Linn, Molecular mechanisms of mammalian DNA repair and the DNA damage checkpoints, Annu Rev Biochem 73 (2004) 39-85.

50. N. Gao, M. Rahmani, P. Dent, S. Grant, 2-Methoxyestradiol-induced apoptosis in human leukemia cells proceeds through a reactive oxygen species and Akt-dependent process, Oncogene 24(23) (2005) 3797-3809.

51. M.R. She, J.G. Li, K.Y. Guo, W. Lin, X. Du, X.Q. Niu, Requirement of reactive oxygen species generation in apoptosis of leukemia cells induced by 2-methoxyestradiol, Acta Pharmacol Sin 28(7) (2007) 1037-1044.

52. Y. Chen, E. McMillan-Ward, J. Kong, S.J. Israels, S.B. Gibson, Oxidative stress induces autophagic cell death independent of apoptosis in transformed and cancer cells, Cell Death Differ 15(1) (2008) 171-182.

53. V.C. Culotta, M. Yang, T.V. O'Halloran, Activation of superoxide dismutases: putting the metal to the pedal, Biochim Biophys Acta 1763(7) (2006) 747-758.

54. R. Kachadourian, S.I. Liochev, D.E. Cabelli, M.N. Patel, I. Fridovich, B.J. Day, 2-methoxyestradiol does not inhibit superoxide dismutase, Arch Biochem Biophys 392(2) (2001) 349-353.

55. P.S. Crooke, M.D. Ritchie, D.L. Hachey, S. Dawling, N. Roodi, F.F. Parl, Estrogens, enzyme variants, and breast cancer: a risk model, Cancer Epidemiol Biomarkers Prev 15(9) (2006) 1620-1629.

56. M. Genestra, Oxyl radicals, redox-sensitive signalling cascades and antioxidants, Cell Signal 19(9) (2007) 1807-1819.

57. M. Djavaheri-Mergny, J. Wietzerbin, F. Besancon, 2-Methoxyestradiol induces apoptosis in Ewing sarcoma cells through mitochondrial hydrogen peroxide production, Oncogene 22(17) (2003) 2558-2567.

58. S. Orrenius, V. Gogvadze, B. Zhivotovsky, Mitochondrial oxidative stress: implications for cell death, Annu Rev Pharmacol Toxicol 47 (2007) 143-183.

59. R. Amendola, M. Cervelli, E. Fratini, F. Polticelli, D.E. Sallustio, P. Mariottini, Spermine metabolism and anticancer therapy, Curr Cancer Drug Targets 9(2) (2009) 118-130.

60. Y. Wang, R.A. Casero, Jr., Mammalian polyamine catabolism: a therapeutic target, a pathological problem, or both?, J Biochem 139(1) (2006) 17-25.

61. A. Pledgie, Y. Huang, A. Hacker, Z. Zhang, P.M. Woster, N.E. Davidson, R.A. Casero, Jr., Spermine oxidase SMO(PAOh1), Not N1-acetylpolyamine oxidase PAO, is the primary source of cytotoxic H2O2 in polyamine analogue-treated human breast cancer cell lines, J Biol Chem 280(48) (2005) 39843-39851.

62. R. Amendola, A. Bellini, M. Cervelli, P. Degan, L. Marcocci, F. Martini, P. Mariottini, Direct oxidative DNA damage, apoptosis and radio sensitivity by spermine oxidase activities in mouse neuroblastoma cells, Biochim Biophys Acta 1755(1) (2005) 15-24.

63. S.M. Keyse, R.M. Tyrrell, Heme oxygenase is the major 32-kDa stress protein induced in human skin fibroblasts by UVA radiation, hydrogen peroxide, and sodium arsenite, Proc Natl Acad Sci U S A 86(1) (1989) 99-103.

64. S.W. Ryter, M. Si, C.C. Lai, C.Y. Su, Regulation of endothelial heme oxygenase activity during hypoxia is dependent on chelatable iron, Am J Physiol Heart Circ Physiol 279(6) (2000) H2889-2897.

65. S.I. Liochev, I. Fridovich, The Haber-Weiss cycle -- 70 years later: an alternative view, Redox Rep 7(1) (2002) 55-57; author reply 59-60.

66. M. Kadowaki, M.R. Karim, A. Carpi, G. Miotto, Nutrient control of macroautophagy in mammalian cells, Mol Aspects Med 27(5-6) (2006) 426-443.

67. M.B. Azad, Y. Chen, S.B. Gibson, Regulation of autophagy by reactive oxygen species (ROS): implications for cancer progression and treatment, Antioxid Redox Signal (2008).

68. N. Hay, The Akt-mTOR tango and its relevance to cancer, Cancer Cell 8(3) (2005) 179-183.

69. C.C. Hudson, M. Liu, G.G. Chiang, D.M. Otterness, D.C. Loomis, F. Kaper, A.J. Giaccia, R.T. Abraham, Regulation of hypoxia-inducible factor 1alpha expression and function by the mammalian target of rapamycin, Mol Cell Biol 22(20) (2002) 7004-7014.

70. B.H. Jiang, L.Z. Liu, PI3K/PTEN signaling in angiogenesis and tumorigenesis, Adv Cancer Res 102 (2009) 19-65.

71. S. Kagawa, J. Gu, T. Honda, T.J. McDonnell, S.G. Swisher, J.A. Roth, B. Fang, Deficiency of caspase-3 in MCF7 cells blocks Bax-mediated nuclear fragmentation but not cell death, Clin Cancer Res 7(5) (2001) 1474-1480.

Figure Captions

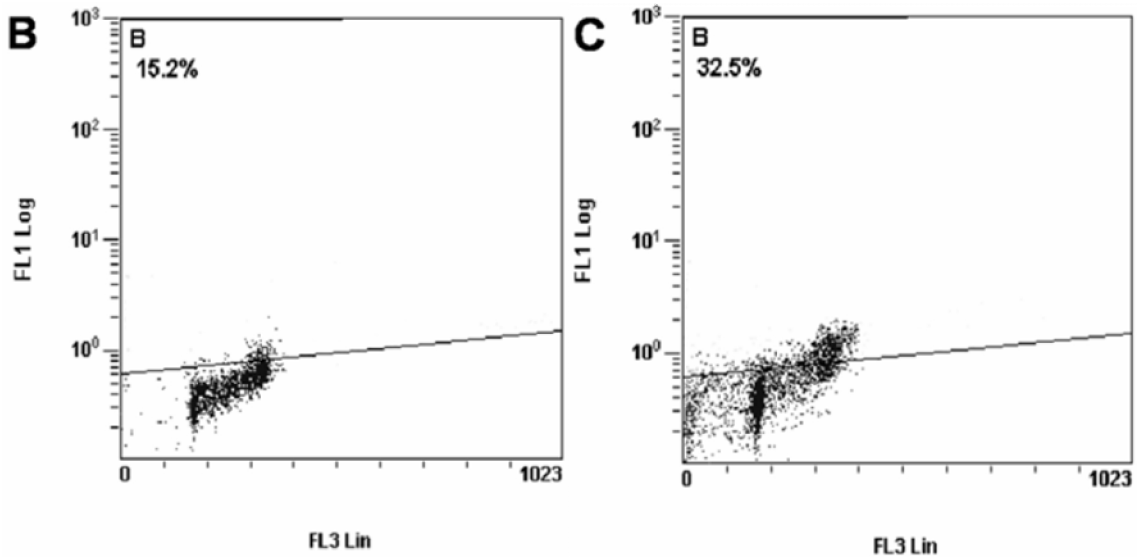

Figure 1: FITC (FL1 Log) vs propidium iodide (FL3 Lin) dot-plot of vehicle-treated cells (A) and 1 µM 2ME-treated (B) MCF-7 cells after 24 h of exposure. FITC-conjugated isotypic control cells where normalized to 2% and subsequent readings were measured on the normalized plot. A marked increase in cyclin B1 levels is observed in the G_2/M fraction of 2ME-treated cells when compared to the vehicle-treated control. Graphs are representative of 3 repeats.

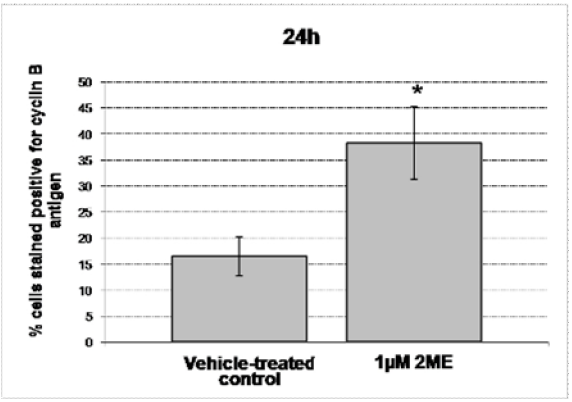

Figure 2: Measurement of cyclin B1 FITC-positive MCF-7 cells. An increase of ±22% to 38±7% in G_2/M cells was observed in 2ME-treated cells when compared to 16±3.7% in vehicle-treated cells. An asterisk (*) indicates a *P*-value < 0.05. Figures are representative of three repeats.

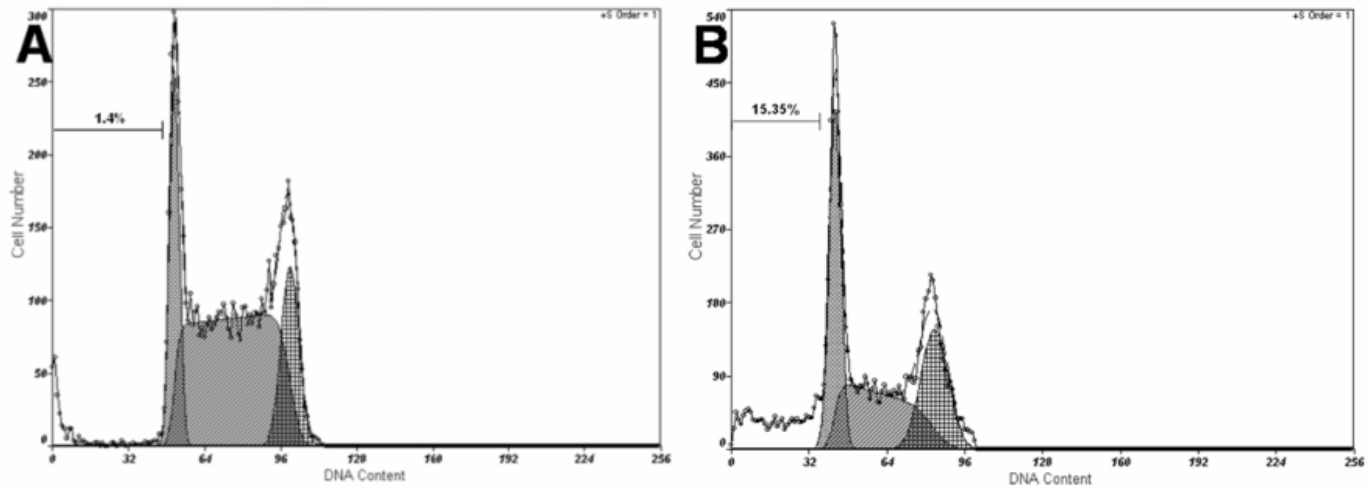

Figure 3: Cell cycle histograms (FL3 Log) of vehicle-treated control cells (A) and 1 μM 2ME-treated (B) MCF-7 cells after 24 h of exposure. A marked increase in the number of cells present in the sub-G_1 fraction is observed in 2ME-treated cells. The S-phase is more pronounced in the vehicle-treated control.

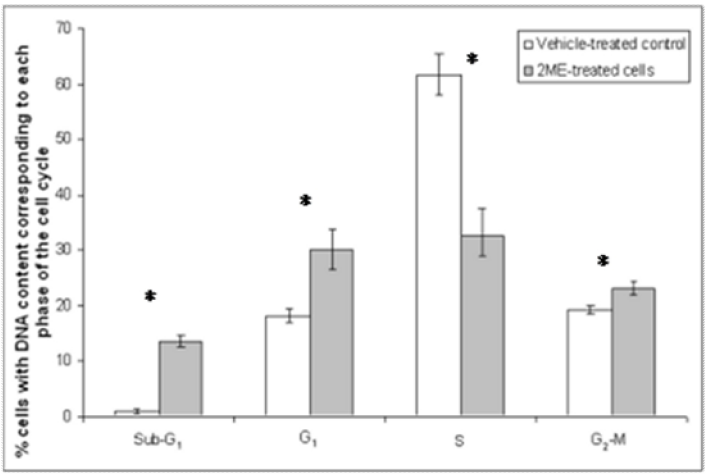

Figure 4: Distribution of DNA content in vehicle-treated and 1 μM 2ME-treated MCF-7 cells. A statistically significant increase in the G_2/M phase in 2ME-treated cells (23.07±1.7%) compared to vehicle-treated cells (19.3±0.9%) is observed. An asterisk (*) indicates a *P*-value < 0.05 when compared to the vehicle control.

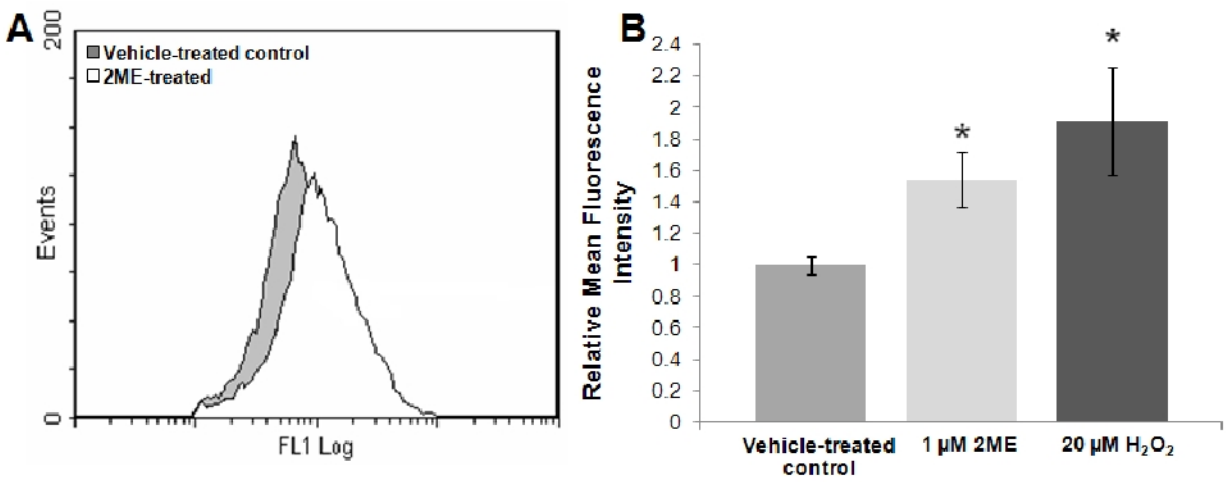

Figure 5: DCFDA (FL1 Log) histogram of 1 µM 2ME-treated cells superimposed on the vehicle-treated control cells (set as control) in MCF-7 cells after 24 h of exposure. An increase in mean DCF fluorescence intensity (shift to the right) is observed in both 2ME-treated (A). B) Relative mean fluorescence intensity of vehicle-treated (normalized to 1), 1 µM 2ME-treated and 20 µM H_2O_2-treated cells. A 1.54±0.17-fold increase (P = 0.004) in mean fluorescence intensity in 2ME-treated cells and a 1.92±0.33-fold increase (P = 0.003) in H_2O_2-treated positive control was observed when compared to the vehicle-treated control. An asterisk (*) indicates a P-value < 0.05 when compared to vehicle control (B).

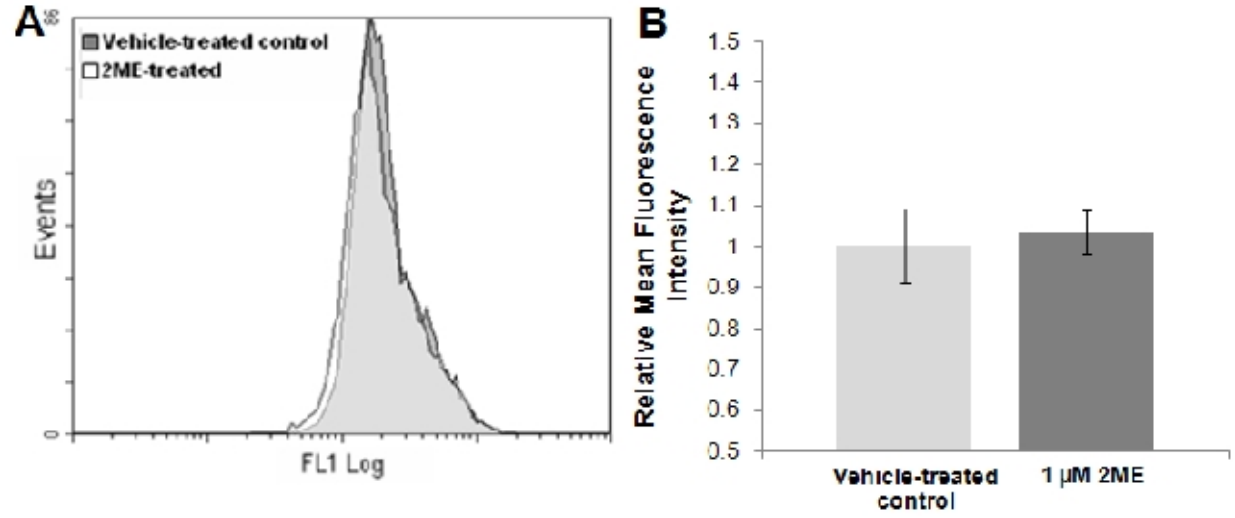

Figure 6: Hydroethidine (FL2 Log) histogram of 1 µM 2ME-treated cells superimposed on the vehicle-treated control cells (set as control) in MCF-7 cells after 24 h of exposure. No significant difference was observed (A). Relative mean fluorescence intensity of vehicle-treated (normalized to 1) and 1 µM 2ME-treated cells. A statistically insignificant (P = 0.6) 1.03-fold increase in mean fluorescence intensity in 2ME-treated cells was observed when compared to the vehicle-treated control (B).

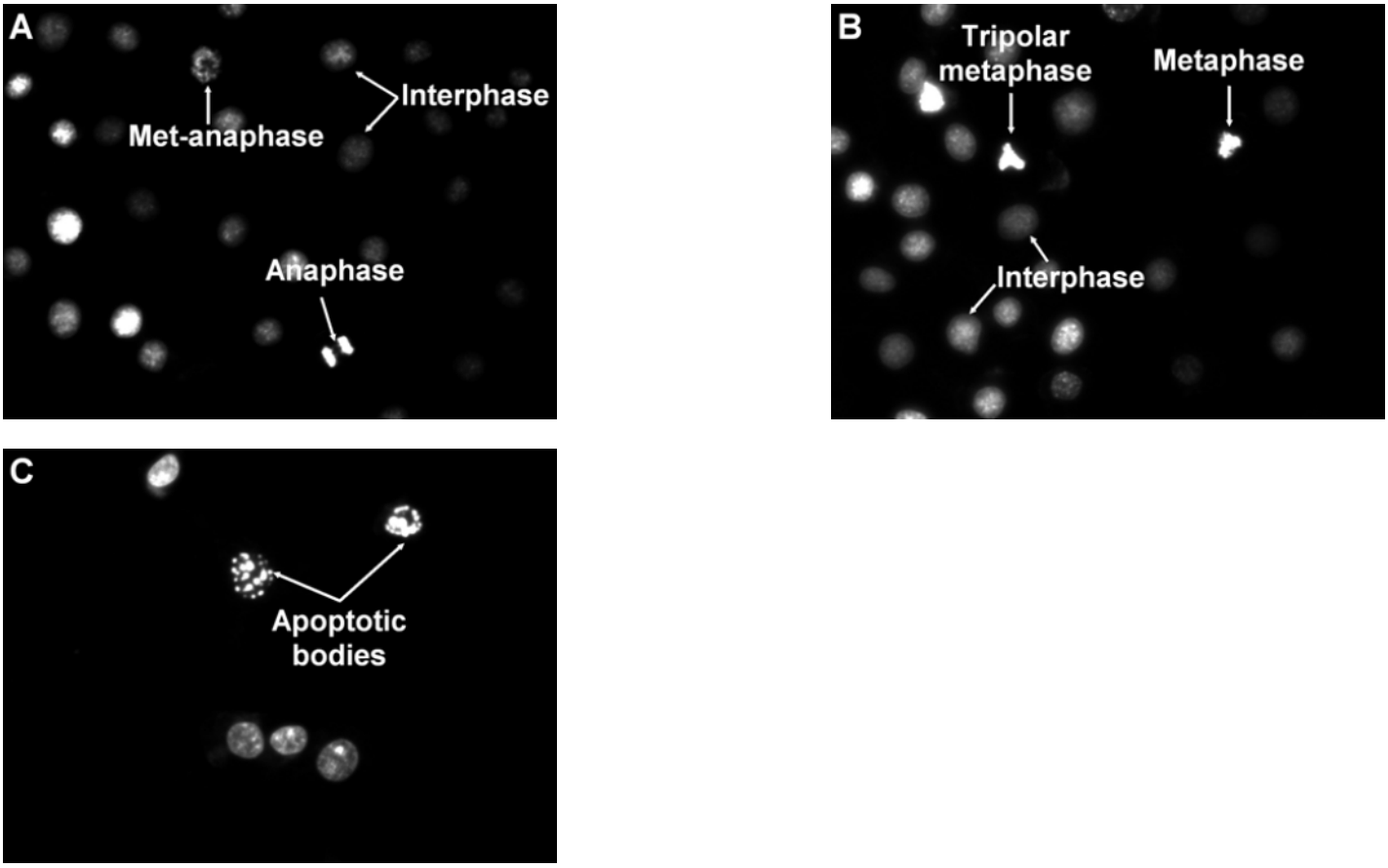

Figure 7: Hoechst 33342-stained vehicle-treated (A), 1 μM 2ME-treated (B) and 0.2 μg/ml Actinomycin D-treated (C) MCF-7 cells after 24 h of exposure. Normal cycling cells in anaphase and met-anaphase are observed in the vehicle-treated control (A). Cells in metaphase and tripolar metaphase are observed in 2ME-treated cells (B). Actinomycin D-treated cells exhibit hallmarks of late stages of apoptosis including hypercondensed chromatin during apoptotic body formation (C).

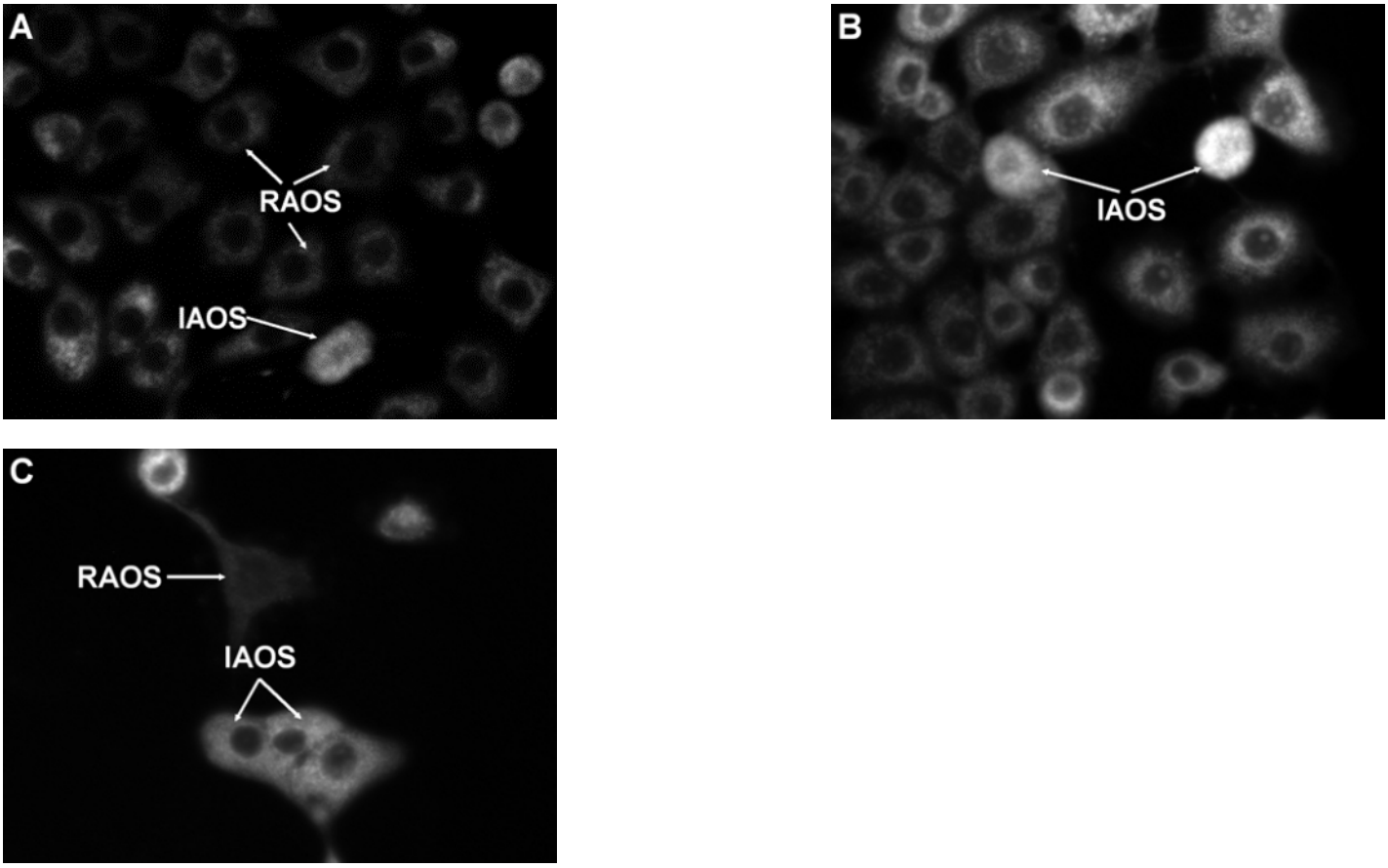

Figure 8: Acridine orange-stained vehicle-treated (A), 1 μM 2ME-treated (B) and 0.2 μg/ml Actinomycin D-treated (C) MCF-7 cells after 24 h of exposure. Residual acridine orange staining (RAOS) is observed vehicle-treated cells. However, an increase in acridine orange staining is also observed in cells undergoing mitosis (A). An overall increase in acridine orange (IAOS) is observed in 2ME-treated cells (B), while cells undergoing late stages of apoptosis in Actinomycin D-treated cells have residual acridine orange staining (C).

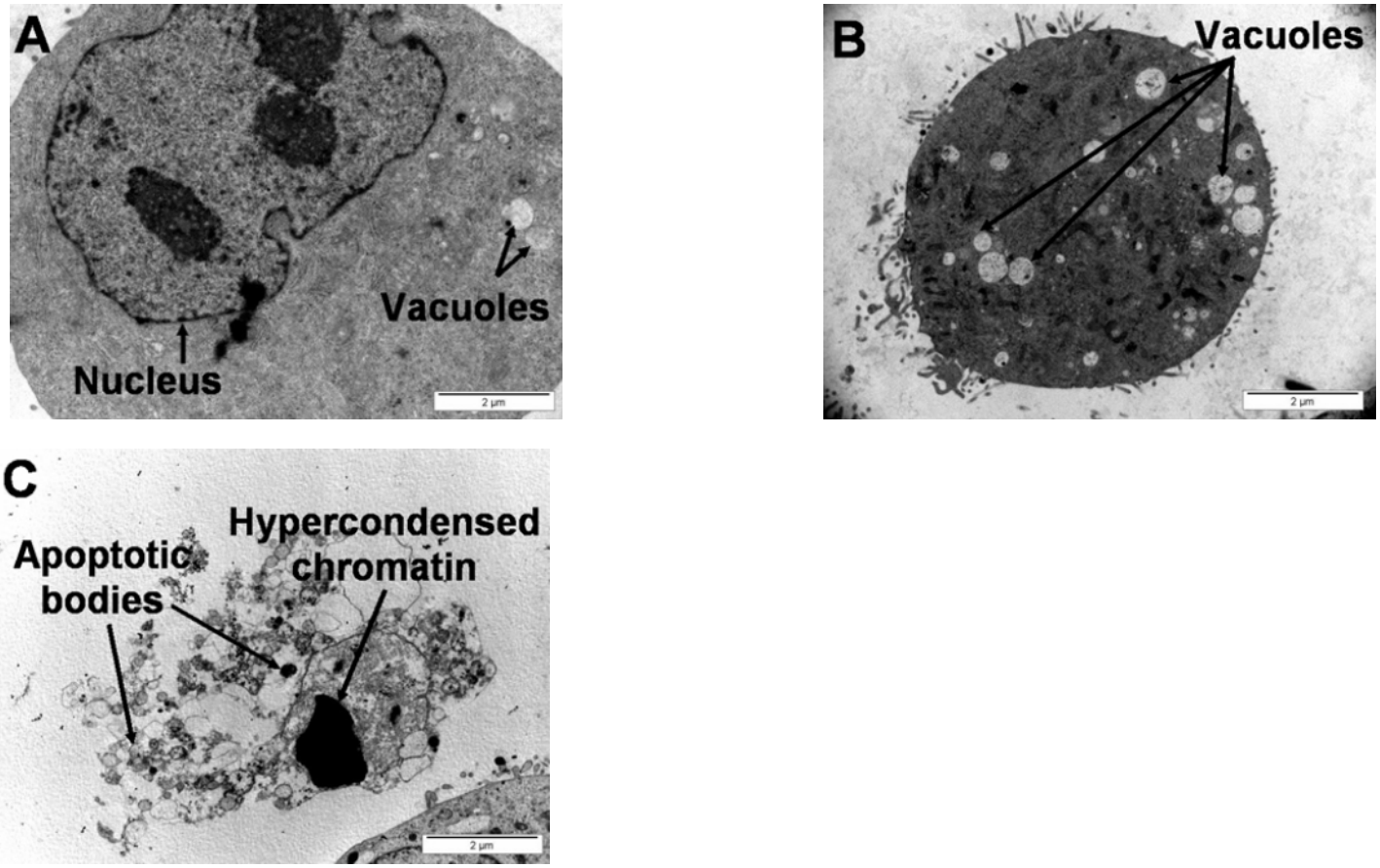

Figure 9: Transmission electron micrographs of MCF-7-stained vehicle-treated (A), 1 µM 2ME-treated (B) and 0.2 µg/ml Actinomycin D-treated (C) MCF-7 cells after 24 h of exposure. Normal nuclear and cytoplasmic physiology is observed in vehicle-treated cells (A). 2ME-treated cells show an increase in the formation of vacuolar structures (B). Formation of apoptotic bodies and hypercondensed chromatin are observed in Actinomycin D-treated cells.

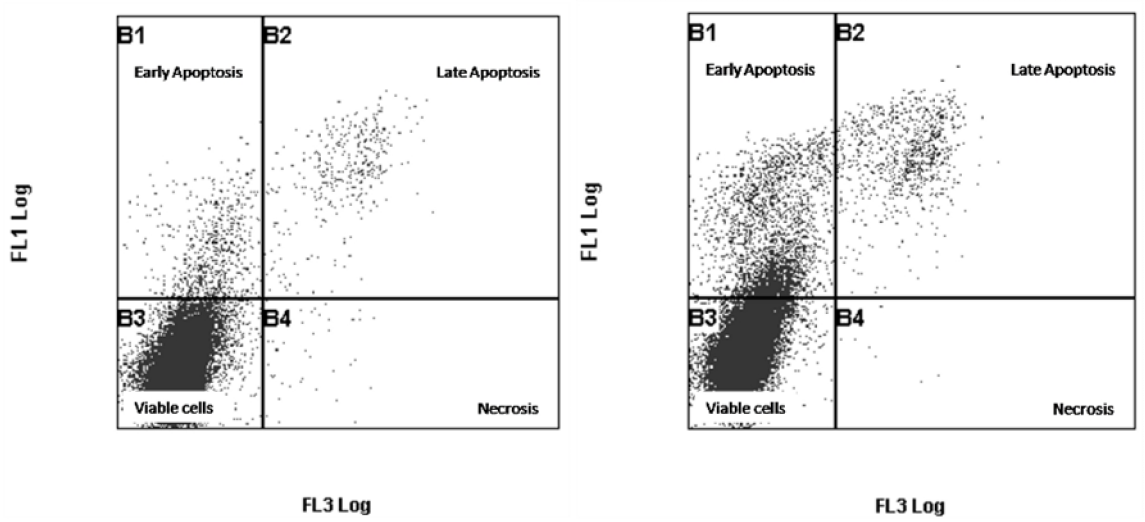

Figure 10: Propidium iodide (FL3 Log) vs Annexin V (FL1 Log) dot-plot of vehicle-treated (A) and 1 µM 2ME-treated (B) MCF-7 cells after 24 h of exposure. 2ME-treated cells show an increase in early and late stages of apoptosis when compared to vehicle-treated cells (A and B).

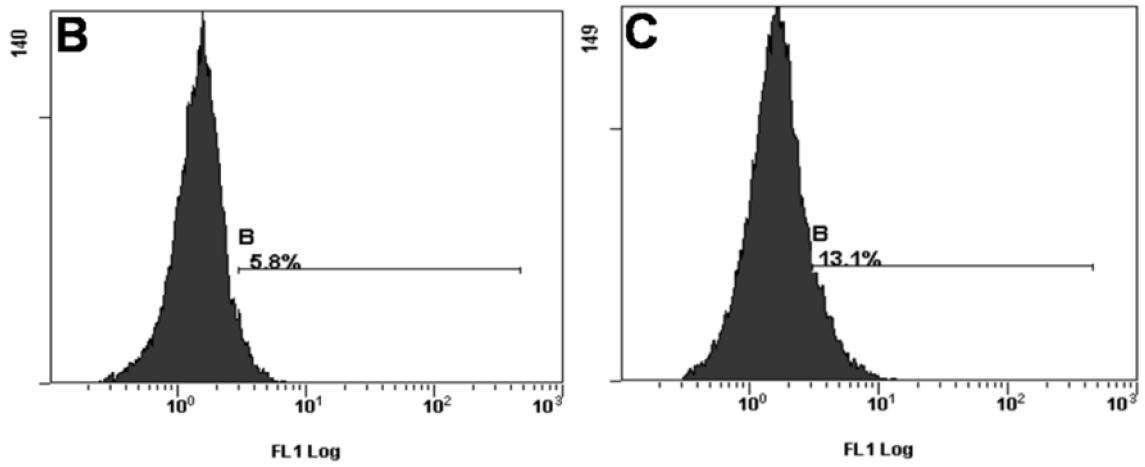

Figure 11: FITC (FL1 Log) histogram vehicle-treated control (A) and 1 µM 2ME-treated (B) MCF-7cells. Intracellular cytochrome *c* levels are slightly increased in 2ME-treated cells when compared to the vehicle-treated control.

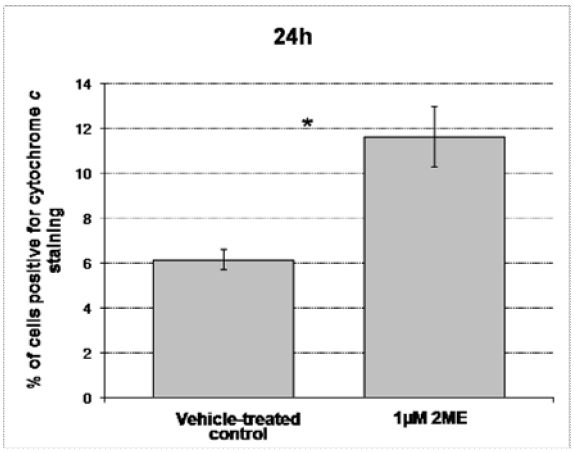

Figure 12: Relative mean fluorescence intensity of vehicle-treated (normalized to 1) and 1 µM 2ME treated MCF-7 cells. 2ME-treated cells exhibited a statistically significant 1.16±0.08-fold increase over the vehicle-treated control (normalized to 1).

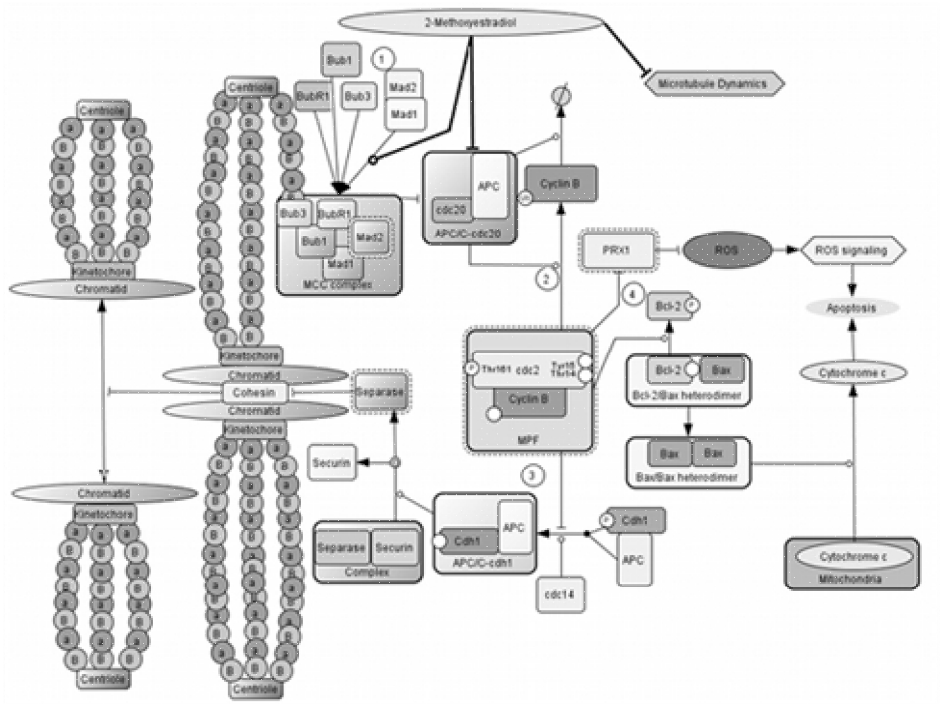

Figure 13: Possible mechanisms of action in 2ME-treated MCF-7 cells. 1) 2ME interferes with microtubule dynamics, resulting in abrogated APC/C-cdc20 activity a result of an active MCC signaling. 2) Decreased cyclin B degradation as a result of APC/C-cdc20 results in prolonged cyclin B/cdc2 activity. 3) Prolonged cyclin B/cdc2 activity inhibits APC/C-cdh1 activity and subsequent cohesion cleavage. 4) Prolonged cyclin B/cdc2 activity inhibits the activity of PRX1, thereby, contributing to ROS formation, resulting in increased and prolonged ROS signaling and subsequent cellular stress signaling cascades associated with growth inhibition and apoptosis.

Table Legends

Table 1: Measurement of phosphatidylserine externalization and membrane permeability of vehicle-treated, 1 µM 2ME-treated and 0.2 µg/ml Actinomycin D-treated MCF-7 cells after 24 h of exposure as an indication of cells in various stages of cell death. An increase in early and late stage of apoptosis was observed in 2ME-treated cells when compared to vehicle-treated cells. Late stages of apoptosis were not as pronounced in 2ME-treated cells when compared to Actinomycin D-treated cells.

(mean %)	Vehicle control	1µM 2-methoxyestradiol
Early apoptosis	2.66	11.14
Late apoptosis	1.52	3.95
Necrosis	0.95	0.34
Viable cells	94.87	84.57

Supplementary Table 1: Selected genes (gene name in brackets) upregulated in 24 h 2ME-treated MCF-7 cells revealed by amplified cRNA microarray and bioinformatics analyses.

Agilent Reference number 44k	Description	log M (Diff expressed) Exposed - Control	*B*-value
	Regulation of Transcription		
45024	Cyclin-dependent kinase inhibitor 2A (CDKN2A) [NM_058197]	1.300	1.284
8598	CCAAT/enhancer binding protein (C/EBP), beta (CEBPB) [NM_005194]	0.474	3.943
15915	CCAAT/enhancer binding protein (C/EBP), beta (CEBPB) [NM_005194]	0.500	4.784
37339	CCAAT/enhancer binding protein (C/EBP), beta (CEBPB) [NM_005194]	0.517	2.244
19214	CCAAT/enhancer binding protein (C/EBP), beta (CEBPB) [NM_005194]	0.524	0.036
38829	CCAAT/enhancer binding protein (C/EBP), beta (CEBPB) [NM_005194]	0.538	4.183
14125	CCAAT/enhancer binding protein (C/EBP), beta (CEBPB) [NM_005194]	0.589	5.911
18594	CCAAT/enhancer binding protein (C/EBP), beta (CEBPB) [NM_005194]	0.594	2.075
14998	CCAAT/enhancer binding protein (C/EBP), beta (CEBPB) [NM_005194]	0.605	4.042
44942	FIIA-alpha/beta-like factor (ALF), transcript variant 2 [NM_172196]	1.078	1.022
31688	Estrogen-related receptor alpha (ESRRA), [NM_004451]	0.395	0.483
9238	Elongation factor, RNA polymerase II, 2 (ELL2), [NM_012081]	1.153	1.751
24662	Jun oncogene (JUN), [NM_002228]	0.696	4.513
3494	Jun oncogene (JUN), [NM_002228]	0.766	1.886
41956	Jun oncogene (JUN), [NM_002228]	0.768	5.459
22066	Jun oncogene (JUN), [NM_002228]	0.769	1.806
33732	Jun oncogene (JUN), [NM_002228]	0.774	4.070
14635	Myeloid/lymphoid or mixed-lineage leukemia (MLL) [AF272382]	0.187	0.490
26483	Nuclear factor (erythroid-derived 2)-like 1 (NFE2L1), [NM_003204]	0.316	2.219
795	BTB and CNC homology 1, basic leucine zipper transcription factor 1 (BACH1), transcript variant 1, [NM_206866]	0.389	0.600
18067	v-Rel reticuloendotheliosis viral oncogene homolog B, (RELB), [NM_006509]	0.533	3.030
42490	Tumor protein p53 (Li-Fraumeni syndrome) (TP53), [NM_000546]	1.656	1.547
42910	Tumor protein p53 (Li-Fraumeni syndrome) (TP53), [NM_000546]	1.799	1.616
40782	Nuclear receptor subfamily 2, group C, member 2 (NR2C2) [BC063441]	0.626	0.967
42912	CCHC-type zinc finger, nucleic acid binding protein (CNBP) [BU618765]	2.033	1.712

24329	GTF2I repeat domain containing 1 (GTF2IRD1), transcript variant 2, [NM_005685]	0.254	1.228
35433	cAMP responsive element binding protein 5 (CREB5), transcript variant 1, [NM_182898]	0.670	2.291
43172	Suppression of tumorigenicity 18 (ST18) [AF074982]	1.602	1.517
5884	Cbp/p300-interacting transactivator, with Glu/Asp-rich carboxy-terminal domain, 2 (CITED2) [AW844496]	0.265	1.848
35727	Catenin (cadherin-associated protein), beta 1, 88kDa (CTNNB1), [NM_001904]	0.254	0.251
	Signal Transduction		
31298	Ephrin-B1 (EFNB1), [NM_004429]	0.305	2.904
31845	Ephrin-B2 (EFNB2), [NM_004093]	0.489	5.298
64	EPH receptor A2 (EPHA2), [NM_004431]	0.313	0.367
33890	EPH receptor A4 (EPHA4), [NM_004438]	1.312	8.536
26852	Guanine nucleotide binding protein (GNAO1), transcript variant 2, [NM_138736]	0.180	0.596
43171	Insulin-like growth factor 1 (somatomedin C) (IGF1), [NM_000618]	1.744	1.594
10824	Mitogen-activated protein kinase 4 (MAPK4) [X59727]	0.264	2.045
33671	Mitogen-activated protein kinase 6 (MAPK6), [NM_002748]	0.238	1.706
9943	MAP kinase interacting serine/threonine kinase 2 (MKNK2), transcript variant 1, [NM_017572]	0.826	1.200
23078	Vascular endothelial growth factor A (VEGFA), transcript variant 1, [NM_001025366]	0.377	3.235
16892	Vascular endothelial growth factor A (VEGFA), transcript variant 1, [NM_001025366]	0.393	2.916
12314	Vascular endothelial growth factor A (VEGFA), transcript variant 1, [NM_001025366]	0.397	1.026
14992	Vascular endothelial growth factor A (VEGFA), transcript variant 1, [NM_001025366]	0.438	4.690
7785	Wingless-type MMTV integration site family, member 5A (WNT5A), [NM_003392]	0.291	1.035
42254	O-linked N-acetylglucosamine (GlcNAc) transferase (OGT), transcript variant 1, [NM_181672]	0.835	1.104
43594	[NM_003810]	1.687	1.564
33081	Dual-specificity tyrosine-(Y)-phosphorylation regulated kinase 3 (DYRK3), transcript variant 2, [NM_001004023]	0.960	6.152
1085	RIO kinase 2 (yeast) (RIOK2), [NM_018343]	0.262	1.120
29835	RIO kinase 2 (yeast) (RIOK2), [NM_018343]	0.291	1.176
8455	RIO kinase 2 (yeast) (RIOK2), [NM_018343]	0.307	2.390
1263	RIO kinase 2 (yeast) (RIOK2), [NM_018343]	0.336	1.651
13570	RIO kinase 2 (yeast) (RIOK2), [NM_018343]	0.342	1.925
18043	RIO kinase 3 (yeast) (RIOK3), transcript variant 2, [NM_145906]	0.750	6.199
8135	Serine/threonine kinase 38 like (STK38L), [NM_015000]	0.355	4.038
13309	Connector enhancer of kinase suppressor of Ras 1 (CNKSR1), [NM_006314]	0.207	0.806
42064	Dual specificity phosphatase 1 (DUSP1), [NM_004417]	1.034	4.180
27432	Protein phosphatase 3 (formerly 2B), regulatory subunit B, 19kDa, alpha isoform (calcineurin B, type I) (PPP3R1), [NM_000945]	0.240	1.976
20674	Phosphatase and tensin homolog (mutated in multiple advanced cancers 1) (PTEN), [NM_000314]	0.184	0.441
24691	Phosphatase and tensin homolog (mutated in multiple advanced cancers 1) (PTEN), [NM_000314]	0.252	0.887

29447	Phosphatase and tensin homolog (mutated in multiple advanced cancers 1) (PTEN), [NM_000314]	0.256	0.259
7808	Phosphatase and tensin homolog (mutated in multiple advanced cancers 1) (PTEN), [NM_000314]	0.263	1.208
2464	HRAS-like suppressor 3 (HRASLS3), [NM_007069]	0.309	0.582
41498	Suppressor of cytokine signaling 3 (SOCS3), [NM_003955]	0.270	1.926
44338	SHC (Src homology 2 domain containing) transforming protein 1 (SHC1), transcript variant 2, [NM_003029]	1.070	1.010
21816	Nemo-like kinase (NLK), [NM_016231]	0.229	0.545
43055	phospholipase A2, group IIF (PLA2G2F), [NM_022819]	0.873	0.721
5444	BAI1-associated protein 2 (BAIAP2), transcript variant 1, [NM_017450]	0.679	3.410
16103	endothelin 1 (EDN1), mRNA [NM_001955]	0.64	5.92
36638	Interleukin 6 (interferon, beta 2) (IL6), mRNA [NM_000600]	1.41	14.90
39120	Interleukin 6 (interferon, beta 2) (IL6), mRNA [NM_000600]	1.45	14.70
10073	Interleukin 6 (interferon, beta 2) (IL6), mRNA [NM_000600]	1.45	10.57
28841	Interleukin 6 (interferon, beta 2) (IL6), mRNA [NM_000600]	1.47	14.93
42277	Interleukin 6 (interferon, beta 2) (IL6), mRNA [NM_000600]	1.49	14.81
14530	Interleukin 6 (interferon, beta 2) (IL6), mRNA [NM_000600]	1.50	11.85
10592	Interleukin 6 (interferon, beta 2) (IL6), mRNA [NM_000600]	1.50	13.78
22295	Interleukin 6 (interferon, beta 2) (IL6), mRNA [NM_000600]	1.52	14.86
32080	Interleukin 6 (interferon, beta 2) (IL6), mRNA [NM_000600]	1.54	14.54
20756	Interleukin 6 (interferon, beta 2) (IL6), mRNA [NM_000600]	1.56	15.30
	Cell Cycle		
45024	Cyclin-dependent kinase inhibitor 2A (CDKN2A) [NM_058197]	1.300	1.284
25725	Septin 1 (SEPT1) [AK056275]	0.526	2.720
43491	Septin 2 (SEPT2), transcript variant 1, [NM_001008491]	1.124	1.085
26120	Spindlin family, member 2B (SPIN2B), transcript variant 3, [NM_001006683]	0.367	2.934
10053	Regulator of G-protein signalling 2, 24kDa (RGS2), [NM_002923]	0.460	2.620
12325	Cell division cycle 40 homolog (S. cerevisiae) (CDC40), [NM_015891]	0.415	3.522
42054	Transducer of ERBB2, 1 (TOB1), [NM_005749]	0.832	2.475
41450	Transducer of ERBB2, 2 (TOB2), [NM_016272]	0.167	0.355
	Apoptosis		
38136	BCL2 binding component 3 (BBC3) (PUMA), [NM_014417]	2.623	7.464
43235	TP53INP1 tumor protein p53 inducible nuclear protein 1 (TP53INP1) [AK001057]	1.154	1.124
15953	Inositol hexaphosphate kinase 2 (IHPK2), transcript variant 3, [NM_001005910]	0.749	2.538
15182	Calpastatin (CAST), transcript variant 1, mRNA [NM_001750]	0.279	2.343

	Nucleosome assembly		
22940	Histone cluster 1, H2bh (HIST1H2BH), [NM_003524]	0.568	5.780
26132	Histone cluster 1, H2bl (HIST1H2BL), [NM_003519]	0.555	4.875
15833	Histone cluster 1, H2bo (HIST1H2BO), [NM_003527]	0.563	5.763
18518	Histone cluster 2, H2aa4 (HIST2H2AA4), [NM_001040874]	0.394	4.031
40397	DOT1-like, histone H3 methyltransferase (S. cerevisiae) (DOT1L), [NM_032482]	0.231	0.506
	Reactive oxygen species metabolism		
18169	Sequestosome 1(SQSTM1), [U46752]	1.239	7.238
43478	Heme oxygenase (decycling) 1 (HMOX1), [NM_002133]	0.418	0.605
42685	Heme oxygenase (decycling) 1 (HMOX1), [NM_002133]	0.437	4.826
40823	Heme oxygenase (decycling) 1 (HMOX1), [NM_002133]	0.462	3.509
20842	Heme oxygenase (decycling) 1 (HMOX1), [NM_002133]	0.517	3.501
29347	Heme oxygenase (decycling) 1 (HMOX1), [NM_002133]	0.550	4.903
28433	Glutathione S-transferase pi (GSTP1), [NM_000852]	0.333	1.710
14586	Cytochrome P450, family 4, subfamily F, polypeptide 8 (CYP4F8)	0.301	2.583
38810	Spermine oxidase (SMOX), [NM_175839]	0.712	4.627

Supplementary Table 2: Selected genes (gene name in brackets) downregulated in 24 h 2ME-treated MCF-7 cells revealed by amplified cRNA microarray and bioinformatics analyses.

Agilent Reference number 44k	Description	log M (Diff expressed) Exposed - Control	*B*-value
	Regulation of Transcription		
32943	PC4 and SFRS1 interacting protein 1 (PSIP1), transcript variant 2, [NM_033222]	-0.419	3.554
5222	PC4 and SFRS1 interacting protein 1 (PSIP1), transcript variant 1, [NM_021144]	-0.372	3.338
24763	E2F transcription factor 1 (E2F1), [NM_005225]	-0.382	0.628
8463	E2F transcription factor 1 (E2F1), [NM_005225]	-0.380	2.232
24063	E2F transcription factor 1 (E2F1), [NM_005225]	-0.357	3.102
40655	E2F transcription factor 1 (E2F1), [NM_005225]	-0.288	2.830
27072	Eukaryotic translation elongation factor 1 alpha 1 (EEF1A1), [NM_001402]	-0.411	2.174
28804	Eukaryotic translation initiation factor 2C, 1 (EIF2C1), [NM_012199]	-0.236	1.189
24898	Eukaryotic translation initiation factor 4A, isoform 2 (EIF4A2), [NM_001967]	-0.269	2.271
2014	Eukaryotic translation initiation factor 3, subunit 6 48kDa (EIF3S6), mRNA [NM_001568]	-0.35	0.34
32368	Eukaryotic translation initiation factor 4B (EIF4B), mRNA [NM_001417]	-0.29	2.11
5425	Eukaryotic translation initiation factor 4E (EIF4E), [NM_001968]	-0.221	1.467
32010	Eukaryotic translation initiation factor 4E (EIF4E), [NM_001968]	-0.178	0.742
41986	Uveal autoantigen with coiled-coil domains and ankyrin repeats (UACA), transcript variant 2, [NM_001008224]	-0.319	3.362
36386	Ubiquitin carboxyl-terminal hydrolase L5 (UCHL5), [NM_015984]	-0.359	0.418
15643	Ubiquitin carboxyl-terminal hydrolase L5 (UCHL5), [NM_015984]	-0.299	0.915
37541	Ubiquitin carboxyl-terminal hydrolase L5 (UCHL5), [NM_015984]	-0.294	2.441
15455	Ubiquitin-like, containing PHD and RING finger domains, 1 (UHRF1), transcript variant 2, [NM_013282]	-0.971	4.684
36133	Ubiquitin specific peptidase 1 (USP1), transcript variant 1, [NM_003368]	-0.668	2.778
14676	Ubiquitin specific peptidase 10 (USP10), [NM_005153]	-0.226	1.210
20127	MCM5 minichromosome maintenance deficient 5, cell division cycle 46 (S. cerevisiae) (MCM5), [NM_006739]	-0.910	5.014
31965	MCM5 minichromosome maintenance deficient 5, cell division cycle 46 (S. cerevisiae) (MCM5), [NM_006739]	-0.813	1.225
41299	v-Myb myeloblastosis viral oncogene homolog (avian)-like 1 (MYBL1) [NM_00108041]	-0.226	0.253
31076	v-Myb myeloblastosis viral oncogene homolog (avian)-like 1 (MYBL1) [NM_00108041]	-0.226	0.932
10057	B-cell CLL/lymphoma 11A (zinc finger protein) (BCL11A), transcript variant 5, [NM_138553]	-0.505	4.373
36848	Methyl-CpG binding domain protein 3 (MBD3), [NM_003926]	-0.153	0.002

22826	Retinoblastoma 1 (including osteosarcoma) (RB1), [NM_000321]	-0.277	1.467
27682	Replication factor C (activator 1) 1, 145kDa (RFC1), [NM_002913]	-0.391	1.398
42983	Replication factor C (activator 1) 4, 37kDa (RFC4), transcript variant 1, [NM_002916]	-0.829	1.303
6967	TAF4 RNA polymerase II, TATA box binding protein (TBP)-associated factor, 135kDa (TAF4), [NM_003185]	-0.329	0.598
44813	Poly(A) binding protein interacting protein 1 (PAIP1), transcript variant 1, [NM_006451]	-0.953	1.219
28023	MYC associated factor X (MAX), transcript variant 3, [NM_145113]	-0.256	0.543
35375	Estrogen-related receptor gamma (ESRRG), transcript variant 2, [NM_206594]	-0.294	3.138
	Signal Transduction		
19167	Dedicator of cytokinesis 1 (DOCK1), [NM_001380]	-0.182	0.840
19556	Fibroblast growth factor 13 (FGF13), transcript variant 1A, [NM_004114]	-0.289	0.176
6311	Insulin receptor substrate 1 (IRS1), [NM_005544]	-0.166	0.175
31718	Inositol 1,3,4-triphosphate 5/6 kinase (ITPK1), [NM_014216]	-0.208	1.427
32151	Nuclear receptor subfamily 2, group F, member 2 (NR2F2), [NM_021005]	-0.251	2.387
12661	Protein kinase C, alpha (PRKCA), [NM_002737]	-0.419	4.473
11864	Serum/glucocorticoid regulated kinase (SGK), [NM_005627]	-0.392	2.215
13333	RAS-like, estrogen-regulated, growth inhibitor (RERG), [NM_032918]	0.208	0.252
	Cell Cycle		
17390	Cyclin-dependent kinase inhibitor 2D (p19, inhibits CDK4) (CDKN2D), transcript variant 1, [NM_001800]	-0.314	3.470
1100	Centromere protein E, 312kDa (CENPE), [NM_001813]	-0.539	1.461
6249	Centromere protein E, 312kDa (CENPE), [NM_001813]	-0.382	0.709
40847	Centromere protein E, 312kDa (CENPE), [NM_001813]	-0.373	3.133
41436	Centromere protein E, 312kDa (CENPE), [NM_001813]	-0.369	3.382
1896	Centromere protein E, 312kDa (CENPE), [NM_001813]	-0.226	1.655
6165	Centromere protein J (CENPJ), [NM_018451]	-0.450	1.365
38539	Centromere protein T (CENPT), [NM_025082]	-0.281	2.771
8545	Centrosomal protein 55kDa (CEP55), [NM_018131]	-0.531	5.301
3846	Abnormal spindle homolog, microcephaly associated (Drosophila) (ASPM), [NM_018136]	-0.408	0.651
24997	Protein phosphatase 1, catalytic subunit, gamma isoform	-0.332	1.282
12005	Anaphase promoting complex subunit 1 (ANAPC1), [NM_022662]	-0.190	0.039
6731	Cyclin A2 (CCNA2), [NM_001237]	-0.541	1.119
566	Cyclin A2 (CCNA2), [NM_001237]	-0.539	2.947
11025	Cyclin B1 (CCNB1), [NM_031966]	-0.390	1.691
38205	Cyclin B2 (CCNB2), [NM_004701]	-0.472	3.490
32992	Cell division cycle 2, G1 to S and G2 to M (CDC2), transcript variant 1, [NM_001786]	-1.640	0.329
4502	Cell division cycle 2, G1 to S and G2 to M (CDC2), transcript variant 1, [NM_001786]	-1.613	3.523
40958	Cell division cycle 2, G1 to S and G2 to M (CDC2), transcript variant 1, [NM_001786]	-1.601	1.180

24761	Cell division cycle 2, G1 to S and G2 to M (CDC2), transcript variant 1, [NM_001786]	-1.589	1.528
30680	Cell division cycle 2, G1 to S and G2 to M (CDC2), transcript variant 1, [NM_001786]	-1.541	1.629
2213	Cell division cycle 2, G1 to S and G2 to M (CDC2), transcript variant 1, [NM_001786]	-1.536	2.151
22913	Cell division cycle 2, G1 to S and G2 to M (CDC2), transcript variant 1, [NM_001786]	-1.520	1.014
6646	Cell division cycle 2, G1 to S and G2 to M (CDC2), transcript variant 1, [NM_001786]	-1.511	3.455
22672	Cell division cycle 20 homolog (S. cerevisiae) (CDC20), [NM_001255]	-0.339	0.759
14751	Protein kinase, membrane associated tyrosine/threonine 1 (PKMYT1), transcript variant 2, [NM_182687]	-0.561	0.358
32202	Nucleolar and spindle associated protein 1 (NUSAP1), transcript variant 1, [NM_016359]	-0.345	1.027
20178	Microspherule protein 1 (MCRS1), transcript variant 1, [NM_006337]	-0.397	1.254
	Apoptosis		
10057	B-cell CLL/lymphoma 11A (zinc finger protein) (BCL11A), transcript variant 5, [NM_138553]	-0.505	4.373
10360	v-Myc myelocytomatosis viral oncogene homolog (avian) (MYC), [NM_002467]	-0.295	3.141
15117	v-Myc myelocytomatosis viral oncogene homolog (avian) (MYC), [NM_002467]	-0.159	0.006
	Nucleosome assembly		
42448	Histone cluster 1, H1b (HIST1H1B), [NM_005322]	-0.446	5.003
21290	Histone cluster 1, H2ae (HIST1H2AE), [NM_021052]	-0.630	1.325
25240	Histone cluster 1, H2ag (HIST1H2AG), [NM_021064]	-0.660	2.151
20103	Histone cluster 1, H2ah (HIST1H2AH), [NM_080596]	-0.556	4.503
34623	Histone cluster 1, H2aj (HIST1H2AJ), [NM_021066]	-0.782	6.340
27286	Histone cluster 1, H2bc (HIST1H2BC), [NM_003526]	-0.901	3.093
37697	Histone cluster 1, H2bd (HIST1H2BD), transcript variant 1, [NM_021063]	-0.791	0.315
16927	Histone cluster 1, H2bj (HIST1H2BJ), [NM_021058]	-0.763	0.979
38808	Histone cluster 1, H3b (HIST1H3B), [NM_003537]	-0.746	7.031
7672	Histone cluster 1, H3d (HIST1H3D), [NM_003530]	-0.765	5.469
33910	Histone cluster 1, H3f (HIST1H3F), [NM_021018]	-0.697	5.136
26742	Histone cluster 1, H3g (HIST1H3G), [NM_003534]	-0.927	2.573
35067	Histone cluster 1, H3h (HIST1H3H), [NM_003536]	-0.427	0.671
17437	Histone cluster 1, H3j (HIST1H3J), [NM_003535]	-0.736	6.035
5363	Histone cluster 1, H4b (HIST1H4B), [NM_003544]	-0.323	1.673
32961	Histone cluster 1, H4i (HIST1H4I), [NM_003495]	-0.659	5.846
36101	Histone cluster 1, H4j (HIST1H4J), [NM_021968]	-0.820	7.122
36856	Histone cluster 2, H2ab (HIST2H2AB), [NM_175065]	-0.429	2.317
13219	Histone cluster 2, H2ac (HIST2H2AC), [NM_003517]	-0.779	3.627
21511	Histone cluster 2, H3, pseudogene 2 (HIST2H3PS2), [NM_001025303]	-1.244	7.362

25899	Histone cluster 2, H3, pseudogene 2 (HIST2H3PS2), [NM_001025303]	-0.345	2.467
16539	Histone cluster 2, H4b (HIST2H4B), [NM_001034077]	-0.610	1.872
7742	Histone cluster 3, H2a (HIST3H2A), [NM_033445]	-0.443	0.594
21369	H2A Histone family, member J (H2AFJ), transcript variant 2, [NM_177925]	-0.375	3.334
37692	H3 Histone, family 3A (H3F3A), [NM_002107]	-0.258	0.082
	DNA repair		
28691	MutY homolog (E. coli) (MUTYH), transcript variant alpha1, [NM_012222]	-0.240	2.191
29787	Ataxia telangiectasia and Rad3 related (ATR), [NM_001184]	-0.534	1.700
37813	Breast cancer 1, early onset (BRCA1), transcript variant BRCA1b, [NM_007295]	-0.565	0.908
32187	Breast cancer 1, early onset (BRCA1), transcript variant BRCA1b, [NM_007295]	-0.433	2.802
29892	Breast cancer 1, early onset (BRCA1), transcript variant BRCA1b, [NM_007295]	-0.421	0.372
8239	Breast cancer 1, early onset (BRCA1), transcript variant BRCA1b, [NM_007295]	-0.420	3.476
36188	Breast cancer 1, early onset (BRCA1), transcript variant BRCA1b, [NM_007295]	-0.393	0.738
1233	Breast cancer 1, early onset (BRCA1), transcript variant BRCA1b, [NM_007295]	-0.384	3.577
17983	Structural maintenance of chromosomes 1A (SMC1A), [NM_006306]	-0.770	4.471
18356	Damage-specific DNA binding protein 1, 127kDa (DDB1), [NM_001923]	-0.179	0.667
29471	Protein phosphatase 3 (formerly 2B), catalytic subunit, beta isoform (calcineurin A beta) (PPP3CB), [NM_021132]	-0.210	1.580
22973	Proliferating cell nuclear antigen (PCNA), transcript variant 1, [NM_002592]	-0.968	2.903
30021	Proliferating cell nuclear antigen (PCNA), transcript variant 1, [NM_002592]	-0.945	1.230
33625	Proliferating cell nuclear antigen (PCNA), transcript variant 1, [NM_002592]	-0.938	4.269
26234	Proliferating cell nuclear antigen (PCNA), transcript variant 1, [NM_002592]	-0.923	5.389
5515	Proliferating cell nuclear antigen (PCNA), transcript variant 1, [NM_002592]	-0.921	2.708
2956	Proliferating cell nuclear antigen (PCNA), transcript variant 1, [NM_002592]	-0.920	5.051
22565	Proliferating cell nuclear antigen (PCNA), transcript variant 1, [NM_002592]	-0.910	6.362
19595	Proliferating cell nuclear antigen (PCNA), transcript variant 1, [NM_002592]	-0.899	5.641
9581	Proliferating cell nuclear antigen (PCNA), transcript variant 1, [NM_002592]	-0.892	3.368
10750	Proliferating cell nuclear antigen (PCNA), transcript variant 1, [NM_002592]	-0.892	2.982
5318	Topoisomerase (DNA) II binding protein 1 (TOPBP1), [NM_007027]	-0.415	1.988
23934	X-ray repair complementing defective repair in Chinese hamster cells 6 (Ku autoantigen, 70kDa) (XRCC6), [NM_001469]	-0.166	0.251
22510	Poly (ADP-ribose) polymerase family, member 1 (PARP1), [NM_001618]	-0.177	0.288
2255	Non-POU domain containing, octamer-binding (NONO), [NM_007363]	-0.313	1.074
36133	Ubiquitin specific peptidase 1 (USP1), transcript variant 1, [NM_003368]	-0.668	2.778
14676	Ubiquitin specific peptidase 10 (USP10), [NM_005153]	-0.226	1.210
19430	Polymerase (DNA directed), delta 1, catalytic subunit 125kDa (POLD1), [NM_002691]	-0.717	0.509
21661	Polymerase (DNA directed), epsilon 3 (p17 subunit) (POLE3), [NM_017443]	-0.587	1.774

32625	RecQ protein-like 4 (RECQL4), [NM_004260]	-0.256	0.667
	Microtubule Dynamics		
35421	BUB3 budding uninhibited by benzimidazoles 3 homolog (yeast) (BUB3), transcript variant 2, [NM_001007793]	-1.095	6.653
22718	BUB3 budding uninhibited by benzimidazoles 3 homolog (yeast) (BUB3), transcript variant 2, [NM_001007793]	-0.880	7.433
6050	BUB3 budding uninhibited by benzimidazoles 3 homolog (yeast) (BUB3), transcript variant 1, [NM_004725]	-0.323	0.778
26919	Echinoderm microtubule associated protein like 4 (EML4), [NM_019063]	-0.392	4.335
32472	Tubulin, alpha 1 (TUBA1), [NM_006000]	-0.481	1.851
15050	Tubulin, alpha 3 (TUBA3), [NM_006009]	-0.789	4.950
20071	Tubulin, alpha 6 (TUBA6), [NM_032704]	-1.151	8.030
24376	Tubulin, alpha 6 (TUBA6), [NM_032704]	-0.871	0.107
41243	Tubulin, alpha 8 (TUBA8), [NM_018943]	-0.475	0.296
21499	Tubulin, beta (TUBB), [NM_178014]	-0.844	4.333
36881	Tubulin, beta (TUBB), [NM_178014]	-0.764	4.013
1048	Tubulin, beta 2A (TUBB2A), [NM_001069]	-0.978	6.265
23995	Tubulin, beta 2C (TUBB2C), [NM_006088]	-1.518	4.671
35905	Tubulin, beta 6 (TUBB6), [NM_032525]	-0.776	3.683
42579	Dynein, cytoplasmic 2, heavy chain 1, (cDNA clone IMAGE:5265846), complete cds. [BC037496]	-0.201	1.240
2757	Microtubule-associated protein 7 (MAP7), [NM_003980]	-0.276	0.196
1100	Centromere protein E, 312kDa (CENPE), [NM_001813]	-0.539	1.461
6249	Centromere protein E, 312kDa (CENPE), [NM_001813]	-0.382	0.709
40847	Centromere protein E, 312kDa (CENPE), [NM_001813]	-0.373	3.133
41436	Centromere protein E, 312kDa (CENPE), [NM_001813]	-0.369	3.382
1896	Centromere protein E, 312kDa (CENPE), [NM_001813]	-0.226	1.655
6165	Centromere protein J (CENPJ), [NM_018451]	-0.450	1.365
38539	Centromere protein T (CENPT), [NM_025082]	-0.281	2.771
8545	Centrosomal protein 55kDa (CEP55), [NM_018131]	-0.531	5.301
8545	Centrosomal protein 55kDa (CEP55), [NM_018131]	-0.531	5.301
972	Spindle pole body component 25 homolog (S. cerevisiae) (SPBC25), [NM_020675]	-0.88056	6.770142
	Cell Adhesion		
11832	Collagen, type XI, alpha 1 (COL11A1), transcript variant B, [NM_080629]	-1.040	2.332
6206	Fibronectin 1 (FN1), transcript variant 1, [NM_212482]	-0.601	0.214
3974	Fibronectin 1 (FN1), transcript variant 1, [NM_212482]	-0.535	3.405
11780	Fibronectin 1 (FN1), transcript variant 1, [NM_212482]	-0.531	0.923
5497	Fibronectin 1 (FN1), transcript variant 1, [NM_212482]	-0.500	2.560

4212	Lysyl oxidase-like 2 (LOXL2), [NM_002318]	-0.405	3.613
33771	Lysyl oxidase-like 2 (LOXL2), [NM_002318]	-0.396	4.257
23135	Lysyl oxidase-like 2 (LOXL2), [NM_002318]	-0.329	3.381
20748	Lysyl oxidase-like 2 (LOXL2), [NM_002318]	-0.306	0.147
29844	Lysyl oxidase-like 2 (LOXL2), [NM_002318]	-0.287	0.880
16031	Lysyl oxidase-like 2 (LOXL2), [NM_002318]	-0.264	2.009
21594	Discoidin domain receptor family, member 2 (DDR2), transcript variant 1, [NM_001014796]	-0.371	1.816
34185	Tenascin XB (TNXB), transcript variant XB, [NM_019105]	-0.261	2.190
	Ribosomal Activity		
42431	Similar to ribosomal protein L28 (LOC402149), [XR_019242]	-0.339	0.381
37069	Mitochondrial ribosomal protein L39 (MRPL39), transcript variant 1, [NM_017446]	-0.325	1.458
14029	Mitochondrial ribosomal protein S6 (MRPS6), [NM_032476]	-0.387	1.359
24937	Ribosomal protein L10 (RPL10), [NM_006013]	-0.321	0.896
7049	Ribosomal protein L10 (RPL10), [NM_006013]	-0.272	0.500
10915	Ribosomal protein L18a (RPL18A), [NM_000980]	-0.280	0.660
9789	Ribosomal protein L18a (RPL18A), [NM_000980]	-0.235	0.647
21544	Ribosomal protein L28 (RPL28), [NM_000991]	-0.258	1.450
6338	Ribosomal protein L32 (RPL32), transcript variant 3, [NM_001007074]	-0.208	1.069
33706	60S ribosomal protein L18a, complete [THC2650296]	-0.245	0.970